fMRI measurement (Vaidya et al., 1998). This leads to a high elimination rate due to excessive motion artifacts: One study enrolling a relatively young childhood sample (6 years and older) rejected 50% of ADHD subjects and 30% of normal control subjects (Durston et al., 2003). This further leads to a skewed distribution of the sample: Since motion problems are generally more severe for patients with hyperactivity, the resulting subject pool might be enriched with mildly and predominantly inattentive type patients (Epstein et al., 2007). Moreover, ADHD children may be withdrawn for various reasons related to their symptoms including refusal to enter the MRI scanner, refusal to begin or finish a run after entering the MRI scanner, inattention such as forgetting task rules, and falling asleep (Yerys et al., 2009).

Alternatively, functional near-infrared spectroscopy (fNIRS) is relatively immune to these problems, and has been successfully adopted in tasks involving body movement (Herrmann et al., 2004, 2005; Hock et al., 1997; Matsuo et al., 2000; Moriai-Izawa et al., 2012; Okamoto et al., 2004b; Shinba et al., 2004; Suto et al., 2004). Moreover, fNIRS offers other advantages including its compact size (useful in confined experimental settings), affordable price, unrestrictiveness and accessibility, serving as a suitable choice for clinically assessing ADHD children. A growing body of fNIRS studies has started to investigate the cortical hemodynamics of ADHD patients (Ehlis et al., 2008; Inoue et al., 2012; Negoro et al., 2010; Schecklmann et al., 2008, 2010; Weber et al., 2005). Most typically, a recent study focusing on Stroop interference revealed that the right prefrontal cortex oxy-Hb increase due to Stroop interference was reduced in ADHD children, suggesting a dysfunction of the area (Jourdan Moser et al., 2009).

The advent of fNIRS raised the possibility of introducing neuroimaging diagnosis in younger ADHD children, and this might further lead to its application in early clinical treatment. The most common treatment for ADHD children is the administration of methylphenidate (MPH), a psychostimulant drug that has been shown to be effective in improving attention and behavior as well as cognition and social function (Spencer, 2004). The behavioral and cognitive characteristics of ADHD are considered to be partly due to dopamine and noradrenaline dysfunction (Wilens, 2008). MPH is considered to inhibit reuptake of catecholamines, including dopamine, by blocking their transporters and to act as a dopamine agonist in the basal ganglia and cerebral cortices (Arnsten, 2006). A recent longitudinal study reported that the use of MPH to treat children and adolescents with ADHD may be conducive to enhancing educational outcomes by reducing the likelihood of disruptive behavior (Biederman et al., 2009). To confer long-term positive effects of treatment and thereby increase the quality of life of ADHD children, early identification of ADHD and appropriate treatment are important. This led us to postulate that fNIRS would be effective in monitoring the effect of MPH in ADHD children, especially for younger children who are difficult to assess in an fMRI environment.

Response inhibition as measured by go/no-go tasks has emerged as one of the principal paradigms for studying ADHD (Aron and Poldrack, 2005). Using this task, it has been clearly demonstrated that children (Beauregard and Levesque, 2006; Derefinko et al., 2008; Durston et al., 2003; Inoue et al., 2012; Ma et al., 2012; Monden et al., 2012; Siniatchkin et al., 2012; Smith et al., 2006; Solanto et al., 2009; Vaidya et al., 1998), adolescents (Schulz et al., 2004; Tamm et al., 2004) and adults (Dibbets et al., 2009; Karch et al., 2010; Mulligan et al., 2011; Sebastian et al., 2012; Vasic et al., in press) with ADHD have response inhibition deficits. An extensive review of functional neuroimaging in healthy adults indicates that widespread regions of the frontal cortex, especially the right inferior frontal gyrus (IFG), are associated with response inhibition (Aron and Poldrack, 2005). Structural neuroimaging in ADHD has fairly consistently indicated gray matter density reductions in the striatum and right IFG (Durston et al., 2004). A former fMRI study on ADHD children with an MPH history reported that MPH increased the activation of the frontal cortices and striatum in go/no-go tasks (Vaidya et al., 1998). The specificity of the implicated brain regions in healthy subjects, as well as functional and structural changes to those regions in ADHD patients, suggests that response inhibition is a good neuro-functional biomarker candidate for ADHD (Aron and Poldrack, 2005).

Thus, using the decrease of IFG activation during a response inhibition task as a potential neuro-functional biomarker for ADHD, we aimed to establish a robust procedure for detecting its recovery with MPH administration. Our initial effort (Monden et al., 2012) was to test whether fNIRS-based diagnosis could be introduced in actual clinical situations. We demonstrated that fNIRS could monitor the cortical hemodynamics of ADHD children (7 to 14 years old) performing a go/no-go task before and 1.5 h after MPH administration, allowing the observation of the acute effect of MPH as a significant increase in the oxy-Hb signal in the right lateral prefrontal cortex. As the monitoring takes only a few minutes, we further showed that the entire process can be implemented within a single-day hospital visit.

However, since that study was optimized for assessing the feasibility of introducing fNIRS as an actual clinical tool that allows the pre- and post-medication comparison to be performed in a single-day hospital visit, a neuro-pharmacological examination of the effects of MPH on ADHD children has yet to be performed. Thus, in the current study, enrolling sixteen ADHD children and age/sex-matched healthy control children, we examined the pharmacological effects of MPH on the cortical hemodynamics of ADHD during a go/no-go task. Subjects received either MPH or a placebo in a randomized, double-blind, placebo-controlled, crossover design. We hypothesized that MPH would modulate hemodynamic responses in the right prefrontal cortex during a go/no-go task while a placebo would not, and assessed this hypothesis using fNIRS. Moreover, we desire to validate the feasibility of introducing fNIRS-based diagnosis of the effects of MPH administration to ADHD children of 6 years old, the earliest age at which the FDA recommends starting MPH administration.

2. Material and methods

2.1. Subjects

Sixteen clinically referred, right-handed Japanese children with a mean age of 8.8 (SD 2.2, range 6–13 years) who met the DSM-IV criteria for ADHD participated in the study (Table 1). The subject group differed from the previous study (Monden et al., 2012). The Wechsler Intelligence Scale of Children—Third Edition (WISC-III) full IQ scores of subjects were all over 70 (mean 90.3, SD 10.0, range 74–110). Sixteen right-handed control subjects were matched with the ADHD subjects according to age (mean 8.9, SD 2.4, range 6–13 years) and gender (10 boys and 6 girls). IQs of controls (mean 111.8, SD 8.7, range 99–135) were significantly ($t=6.40$, $p<0.0001$) higher than those of ADHD subjects. Written consent was obtained from the parents of all subjects. The study was approved by the Ethics Committees of Jichi Medical University Hospital, and the International University of Health and Welfare. The study was in accordance with the latest version of the Declaration of Helsinki. This study was registered to UMIN-CTR Clinical Trial (UMIN000006277) as "Neurophysiological analysis in developmental disorders: an exploratory neuroimaging study using functional near-infrared spectroscopy (fNIRS)".

2.2. Experimental design

The effects of MPH were examined in a randomized, double-blind, placebo-controlled, crossover study while the subjects performed a go/no-go task. Experimental procedure is summarized in Fig. 1. ADHD subjects were examined twice (the times of day for both measurements were scheduled to be as close as possible), at least 4 days apart, but within 30 days. Control subjects only underwent a pre-administration session.

On each examination day, ADHD subjects underwent two sessions, one before drug (MPH or placebo) administration, and the other at 1.5 h after the drug administration. Each session consisted of 6 block

Table 1
Demographic and clinical profiles for ADHD subjects.

ID	Age (years)	Sex	ADHD subtype	Complication	WISC-III full IQ	MPH dose (mg)	Duration of MPH exposure (years)	Other medications
1	7	M	Inattentive	None	110	18	1.0	None
2	8	M	Combined	None	95	27	1.0	None
3	12	M	Combined	PDD	96	27	1.8	None
4	11	M	Combined	None	82	27	3.4	None
5	6	F	Hyperactive	None	98	18	0.6	None
6	7	M	Combined	PDD	79	18	Naïve	None
7	13	M	Combined	None	82	45	2.1	Carbamazepine, risperidone
8	8	F	Combined	PDD	85	18	Naïve	None
9	8	F	Combined	Epilepsy	85	18	Naïve	Valproic acid
10	8	M	Combined	PDD	101	18	2.0	None
11	8	M	Combined	None	90	27	2.2	None
12	7	M	Combined	None	95	18	Naïve	None
13	6	F	Inattentive	None	74	18	Naïve	None
14	10	M	Combined	None	105	18	Naïve	None
15	9	M	Combined	None	85	18	Naïve	None
16	12	M	Combined	None	90	18	0.1	None
Mean	8.8				90.8			
SD	2.2				9.9			

Abbreviations: SD, standard deviation; PDD: pervasive developmental disorders.

sets, each containing alternating go (baseline) and go/no-go (target) blocks. Each block lasted 24 s and was preceded by instructions displayed for 3 s, giving an overall block-set time of 54 s and a total session time of 5.5 min. In the go block, subjects were presented a random sequence of two pictures and asked to press a button for both pictures. In the go/no-go block, subjects were presented with a no-go picture 50% of the time, thus being required to respond to half the trials (go trials) and inhibit their response to the other half (no-go trials). A go/no-go ratio of 50% was selected as it has been most often used in former neuroimaging studies (Dillo et al., 2010; Herrmann et al., 2005; Liddle et al., 2001; Menon et al., 2001; Vaidya et al., 1998). Pictures were presented with 1 Hz frequency during go and go/no-go blocks. At the beginning of each block, instructions (e.g., "press for tiger or elephant" for go conditions and "do not press for giraffe" for go/no-go conditions) were displayed for 3 s to inform the subject about the new block. Each subject performed a practice block before any measurements to ensure their understanding of the instructions.

After ADHD subjects performed the first session, either MPH (OROS-methylphenidate or Concerta) or a placebo was administered orally. Specific acute doses were the same as their daily dose as described in Table 1.

2.3. fNIRS measurements

We used the multichannel fNIRS system ETG-4000 (Hitachi Medical Corporation, Kashiwa, Japan), using two wavelengths of near-infrared light (695 and 830 nm). We analyzed the optical data based on the modified Beer–Lambert Law (Cope et al., 1988) as previously described (Maki et al., 1995).

We set the fNIRS probes to cover the lateral prefrontal cortices in reference to previous studies (Garavan et al., 1999; Herrmann et al., 2004, 2005; Liddle et al., 2001; Monden et al., 2012; Rubia et al., 2003), resulting in 22 channels (CH) per hemisphere. The specific setting was as previously described (Monden et al., 2012). After the fNIRS measurement, positional data of illuminators and detectors were obtained for both the ADHD and control subjects using a 3D-digitizer (Fastscan, Polhemus), and subjected to probabilistic registration of fNIRS channel positions to MNI space (Jurcak et al., 2007; Okamoto et al., 2004a; Okamoto and Dan, 2005; Singh et al., 2005; Tsuzuki et al., 2007, 2012) with reference to macroanatomical brain atlases (Rorden and Brett, 2000; Shattuck et al., 2008).

Oxy-Hb signals were used for further analysis due to its higher signal amplitude than that of deoxy-Hb (Strangman et al., 2002). Individual timeline data for the oxy-Hb signals of each channel were preprocessed with a first-degree polynomial fitting and high-pass filter using cut-off frequencies of 0.01 Hz to remove baseline drift, and a 0.8 Hz low-pass filter to remove heartbeat pulsations. After removal of blocks with marked motion-related artifacts, timeline data of the remaining blocks (where more than 4 blocks remained) were used. From the preprocessed time series data, we obtained channel-wise and subject-wise contrasts by calculating the inter-block means of difference between the target (4–24 s after go/no-go block onset) and baseline (14–24 s after go block onset) periods.

2.4. Statistical analyses

We performed statistical analyses in a channel-wise manner on oxy-Hb signals. Specifically, for control subjects who were examined only once, the target vs. baseline contrast of the session was generated. For ADHD subjects, the following contrasts were generated: (1) first-day, pre-medication contrast: target vs. baseline contrast for the pre-medication condition (either placebo or MPH administration) for the first day exclusively; (2) pre-medication contrasts: target vs. baseline contrast for the pre-placebo and pre-MPH conditions (for either first or second day measurements); (3) post-medication contrasts (specifically, post-placebo and post-MPH contrasts): target vs. baseline contrast for the post-placebo and post-MPH conditions; (4) intra-medication contrasts: difference between post- and pre-medication contrast for each medication (i.e., intra-placebo and intra-MPH contrasts); and (5) inter-medication contrast: difference between intra-MPH and intra-placebo contrasts. Note that (2) and (4) were generated temporally for calculating (5).

To screen the channels involved in go/no-go tasks in normal control subjects, target vs. baseline contrasts were subjected to one-sample *t*-tests against zero (two-tails). Statistical threshold was set at 0.05 with Bonferroni method for family-wise error correction. For thus-screened channels, comparisons between control and ADHD were performed for the following three ADHD contrasts: (1) first-day, pre-medication, (2) post-placebo, and (3) post-MPH. They were subjected to independent two-sample *t*-tests (two-tails) with a statistical threshold of $p<0.05$. For examining medication effects on ADHD subjects, comparison between intra-MPH and intra-placebo (i.e., inter-medication contrast) was subjected to one-sample *t*-tests against zero (two-tails) with a statistical threshold of $p<0.05$.

2.5. Behavioral data analysis

The reaction time (RT) of go trials, and accuracy (ACC) for go and no-go trials were computed for each go/no-go block. ACCs and RTs were averaged across go/no-go blocks, and subjected to statistical

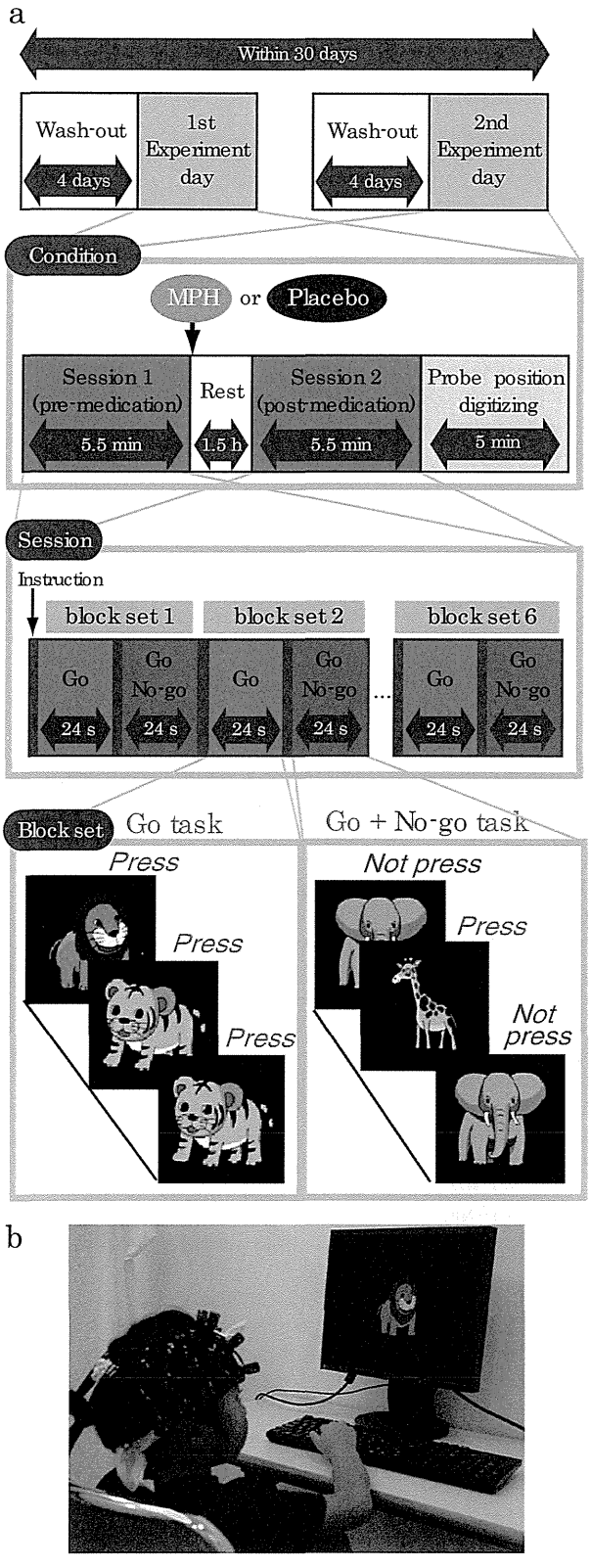

Fig. 1. Experimental design. a. A schematic showing the flow of pre- and post-medication administration sessions for ADHD subjects. b. fNIRS measurements. Brain activity was measured while ADHD and control subjects performed the go/no-go task.

analyses as described in the previous section. Statistical threshold was set at 0.05 with Bonferroni method for multiple-comparison error correction (i.e., significant p was b 0.05/3).

3. Results

3.1. Behavioral performance

The average ACC for go and no-go trials and RT for correct go trials in the go/no-go block for control and ADHD subjects are summarized in Table 2. In ADHD subjects, the first-day data before administration of either a placebo or MPH was used as a representation of pre-medication contrast. Second-day data was excluded for this contrast.

First-day pre-medication, post-placebo, and post-MPH values of ADHD subjects were compared with values for control subjects (Table 2). Significant differences in ACC for no-go trials were found between control subjects and first-day pre-medication ADHD subjects and between control subjects and post-placebo ADHD subjects.

For analysis within each ADHD subject, the inter medication contrast comparing the effect of MPH against the placebo revealed no significant differences in behavioral parameters (Table 3).

3.2. fNIRS analyses

We screened for any fNIRS channels involved in the go/no-go task for the control subjects. Significant oxyHb increase was found in the right CH 10 (mean 0.075, SD 0.074, p b 0.05, Bonferroni-corrected, Cohen's d = 1.009). This channel was located in the border region between the right MFG and IFG (MNI coordinates x,y,z (SD): 46,43,30 (14), MFG 78%, IFG 22% with reference to macroanatomical brain atlases (Rorden and Brett, 2000; Shattuck et al., 2008)). Thus, we set the right CH 10 as a region-of-interest (ROI) for the rest of the study. For reference, cortical activation patterns with all the channels are presented for control and ADHD subjects as supplementary material.

Comparison between oxy-Hb signals of the control and first-day pre-medicated ADHD subjects revealed significantly higher oxy-Hb signal in the right CH 10 in the control subjects (independent two-sample t-test, p b 0.05, Cohen's d = 0.839, Table 2). This indicates that the control subjects exhibited higher right prefrontal activation during go/no-go tasks than did the pre-medicated ADHD children.

Effects of medications were examined between control and post-placebo ADHD subjects, and between control and post-MPH ADHD subjects (independent two-sample t-test, thresholded at p b 0.05). Oxy-Hb signal in control was significantly higher than in post-placebo ADHD subjects, whereas no significant difference was found for those in control and post-MPH ADHD subjects (Table 2). This suggests that the impaired right prefrontal activation in pre-medicated ADHD subjects was normalized by the MPH administration.

Finally, we tested whether there was an MPH-induced, but not placebo-induced, right prefrontal activation in ADHD children. In the inter-medication contrast, the right CH 10 was found to be significant with a large effect size (one-sample t-test, p b 0.05, Cohen's d = 0.952, Table 3). This result indicates that the oxy-Hb signal increase during go/no-go tasks was induced by MPH but not by the placebo.

3.3. Oxy-Hb timeline data

Fig. 2 illustrates the grand average waveforms of all 16 control subjects and 16 ADHD subjects. For ADHD, oxy-Hb and deoxy-Hb signals are presented for pre-/post-placebo and pre-/post-MPH conditions on CH 10 of the right hemisphere. We observed more stable task-related oxy-Hb signals than deoxy-Hb signals, suggesting the robustness of oxy-Hb signals for our experimental conditions. An oxy-Hb increase in the right CH 10 was clearly observed for control and post-MPH administration of ADHD in the grand average waveform. Waveforms for individual subjects (subject 5: 6-year-old ADHD girl, and subject 1: 7-year-old ADHD boy) are also illustrated. Although the individual data resulted in somewhat noisy waveforms,

Table 2
Go/no-go task performance and functional data for control and ADHD subjects.

	Control		ADHD									
			1st day pre-medication				Post-placebo				Post-MPH			
	Mean	SD	Mean	SD	t	p	Mean	SD	t	p	Mean	SD	t	p
ACC for go trials (%)	96.5	5.48	86.2	21.9	1.829	0.085^{ns}	85.3	20.2	2.14	0.047^{ns}	92.3	12.0	1.266	0.219^{ns}
ACC for no-go trials (%)	95.2	4.52	86.6	11.9	2.688	0.014^{*}	86.5	8.46	3.634	0.001^{**}	89.5	8.51	2.347	0.028^{ns}
RT for correct go trials (ms)	421.4	57.5	385.5	96.8	1.275	0.214^{ns}	377.0	83.6	1.753	0.091^{ns}	404.9	47.9	0.881	0.386^{ns}
Oxy-Hb right CH10 (mM·mm)	0.075	0.074	0.008	0.084	2.374	0.024^{*}	0.001	0.087	2.586	0.015^{*}	0.077	0.060	−0.110	0.916^{ns}

Performance data (ACC and RT) is presented for go and no-go trial data from go/no-go blocks. Oxy-Hb values for right CH10 are presented as functional data. For ADHD subjects, data for 1st day pre-medication, post-medication of placebo and MPH are shown. t-value, p-value and statistical significance were the results of t-tests between control and each ADHD condition. Abbreviations: SD, standard deviation; t, t-value; p, p-value. Statistical significances are presented as follows: *, $p<0.05$; **, $p<0.01$; and ns, not significant.

the oxy-Hb activation in the post-MPH session is clearly presented even in the data of the 6-year-old ADHD subject.

3.4. Examination on the effects of IQ

Since we did not match the IQ of the ADHD and normal healthy control subjects, we performed additional analyses to find the possible effects of IQ. We examined the correlation between IQ and activation in the right CH 10 for ADHD children (ADHD 1st day pre-medication contrast) and normal healthy control children, respectively. In ADHD children, Pearson's correlation coefficient was 0.184 ($p=0.494$), while that in control children was 0.010 ($p=0.969$): Neither analysis yielded any significant correlation with a meaningful effect size. In addition, we examined whether the two correlation coefficients were different, but did not find any significant difference (Fischer's $z=0.45$, $p>0.05$). Thus we concluded there was no correlation between IQ and the activation in the right CH 10 in either group.

4. Discussion

The current study exploring fNIRS-based diagnosis of the effects of MPH administered to ADHD children revealed that the right IFG/MFG activation could serve as an objective neuro-functional biomarker for fNIRS measurement. First, relative to control subjects, unmedicated ADHD children exhibited reduced brain activation in the right IFG/MFG during go/no-go task blocks. Second, the reduced right IFG/MFG activation was acutely normalized after MPH administration, but not after placebo administration. Third, the MPH-induced right IFG/MFG activation was significantly larger than the placebo-induced activation.

4.1. Behavioral performance for go/no-go task

The current fNIRS analyses adopted the contrast of go/no-go against go tasks. In addition to response inhibition, this contrast is thought to commeasure additional cognitive functions, including decision making, response competition/response selection, conflict monitoring, and increased attentional demand (Liddle et al., 2001; Menon et al., 2001; Rubia et al., 2001, 2003). Thus, the fNIRS results are expected to reflect a rather wide spectrum of cognitive functions associated with ADHD. On the other hand, neuropsychological tests are expected to examine specific cognitive aspects of ADHD symptoms. Go errors (omission errors) are typically considered indicators of inattention to the task, while no-go errors (commission errors) and RT to go responses are considered indicators of impulsivity (Barkley, 1991; Newcorn et al., 2001). Numerous studies have demonstrated that MPH improves no-go indices in child and adult ADHD patients (Aron et al., 2003; Aron and Poldrack, 2005; Bedard et al., 2003; Tannock et al., 1995). However, MPH also affects the speed of go responses, go response variability, and discrimination errors in go trials (Aron and Poldrack, 2005; Bedard et al., 2003; Tannock et al., 1995). Moreover, Rubia et al. suggested that the beneficial MPH effects were more pronounced for inattention problems (reflected by omission errors) than impulsivity (reflected by commission errors) (Rubia et al., 2009).

In the current study, the comparison between controls and unmedicated ADHD patients showed a significantly higher commission

Table 3
ADHD inter-medication (placebo vs. MPH) comparison.

	Mean	SD	t	p
ACC for go trials (%)	1.98	8.12	0.975	0.345^{ns}
ACC for no-go trials (%)	0.03	11.2	0.011	0.991^{ns}
RT for correct go trials (ms)	0.84	54.3	0.062	0.951^{ns}
Oxy-Hb right CH10 (mM·mm)	0.084	0.088	3.809	0.002^{**}

Abbreviations: SD, standard deviation; t, t-value; p, p-value. Statistical significances are presented as follows: *, $p<0.05$; **, $p<0.01$; and ns, not significant.

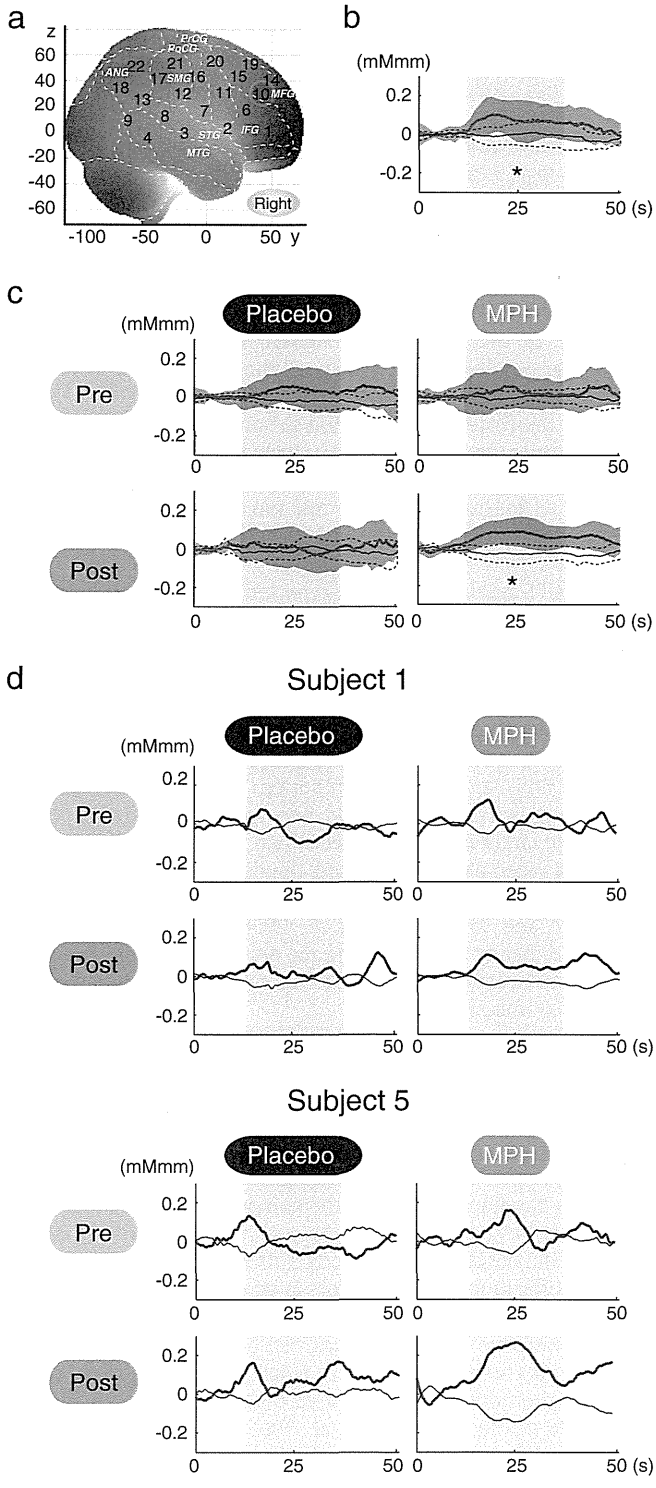

Fig. 2. The channel location and waveforms of oxy-Hb (red line) and deoxy-Hb (blue line) signals for right CH 10. The green area indicates the go/no-go task period. Significant (one-sample *t*-test, $p<.05$) conditions are indicated by asterisks. a. On-brain channel locations (right hemisphere) are statistically estimated for the group of subjects (including both ADHD and control) and exhibited in MNI space. CH 10 is indicated in red. b. Grand averages for control subjects. Standard deviations among the 16 subjects are exhibited as pale red (oxy-Hb) and blue dotted (deoxy-Hb) areas. Each time line is adjusted to the average value for a baseline period of zero. Oxy-Hb and deoxy-Hb signals are shown in units of mM·mm. c. Grand averages for ADHD subjects for pre-/post- and placebo/MPH conditions are illustrated. d. Graphs for ADHD individuals for pre-/post- and placebo/MPH conditions. Subject 1 is a 7-year-old boy and subject 5 is a 6-year-old girl (corresponding to Table 1).

error rate for ADHD subjects. This result was mostly in line with former studies. We detected no significant behavioral performance differences in the MPH-medicated ADHD children contrasted against control subjects, suggesting an MPH effect for no-go performance. However, the inter-condition contrast representing MPH effects against placebo failed to yield any significant behavioral performance change. Although behavioral parameters may often well reflect specific cognitive aspects of ADHD symptoms or MPH effects on them, the current study could not confirm a normalization effect of MPH (but not placebo) on behavioral parameters.

4.2. Right IFG/MFG activation as a robust neuro-functional biomarker

On the other hand, fNIRS may provide more robust measures of MPH effects. Previous neuroimaging studies have elucidated the neural correlates of go/no-go tasks (Simmonds et al., 2008), including the bilateral IFG, MFG and SFG (superior frontal gyrus), supplementary motor area, anterior cingulate gyrus, inferior parietal and temporal lobes, caudate nucleus, and cerebellum (Rubia et al., 2003). The IFG may be specifically related to motor response inhibition, while the MFG/SFG, medial prefrontal, and parietal cortices possibly mediate more general meta-motor executive control functions such as motor attention, conflict monitoring, and response selection, necessary for inhibition task performance (Rubia et al., 2001).

Among these regions, our fNIRS measurements covered the right and left IFG (BA 44/45), MFG (BA 46/9), and SMG (supramarginal gyrus, BA40), and we found activation in the right MFG and IFG (BA9, 46, 45) during the go/no-go task period in the control subjects, but not in the first-day, pre-medicated ADHD subjects. These results suggest that the right prefrontal function associated with the go/no-go task performance was impaired in ADHD children. The administration of a placebo did not result in right prefrontal activation, while that of MPH led the ADHD children to exhibit a degree of right prefrontal activation comparable to that of the normal control subjects. Moreover, the right prefrontal activation due to MPH administration was significantly higher than that due to placebo administration. These results led us to conclude that MPH had significant effects in normalizing right frontal dysfunctions in ADHD children.

The right prefrontal dysfunction and MPH-elicited recovery observed by fNIRS are consistent with former studies using other neuroimaging modalities. A recent ALE meta-analysis of go/no-go tasks (Buchsbaum et al., 2005) reported a mainly right-lateralized network associated with response inhibition, including the right MFG and IFG (BA46/44), the right SMG (BA40), and the superior medial frontal gyrus (BA6) (Simmonds et al., 2008). These regions have been implicated in the processes of stimulus recognition, maintenance and manipulation of stimulus–response associations and response selection, including selecting not to respond (Grafton et al., 1992; Law et al., 1997; Liddle et al., 2001; Mostofsky et al., 2003; Rubia et al., 2001), all of which are critical to the performance of go/no-go tasks (Simmonds et al., 2008). fMRI studies of the go/no-go task have consistently recruited frontal cortices; however, localization and the extent of frontal activation vary across these studies, with activation most often localized to the right IFG (BA 45/47) (Durston et al., 2002; Garavan et al., 1999; Konishi et al., 1999; Rubia et al., 2001), followed by the right MFG/SFG (BA9/46) (Garavan et al., 1999, 2002, 2003, 2006; Hester et al., 2004; Mostofsky and Simmonds, 2008). An fNIRS study also added further evidence to the involvement of the right lateral prefrontal cortex (more exactly, F4) during go/no-go tasks (Boecker et al., 2007). Another recent fNIRS study reported reduced prefrontal activation in ADHD children compared to normal controls during a go/no-go condition (albeit no laterality was reported) (Inoue et al., 2012). Moreover, recent fMRI studies on MPH-medicated children have provided more direct evidence for cortical activation and MPH treatment. Using a continuous performance task, Rubia et al. (2009) found that MPH treatment improved underactivation in ADHD children compared to normal children by adding

activation in the right IFG and MFG along with several other regions (Monden et al., 2012). Therefore, it would be relevant to suggest that normalized right IFG/MFG activation induced by MPH administration during go/no-go task serves as a robust neuro-functional biomarker for fNIRS assessment of MPH effect on ADHD children.

4.3. Effects of IQ

We did not match the IQs of ADHD and normal healthy control children. However, this did not seem to cause any serious effects on the findings of the current study, as we did not find any correlation between IQ and the activation in the right CH 10 in either group. There have been arguments over whether to match IQ or not in ADHD studies. The IQs of ADHD children are lower than those of normal healthy children (Frazier et al., 2004; Kuntsi et al., 2004), and an extensive epidemiological study reported that the co-occurrence of ADHD and low IQ has a genetic overlap (de Zeeuw et al., 2012). Therefore, it is not considered appropriate to treat IQ as a covariant of ANCOVA type of studies (de Zeeuw et al., 2012; Dennis et al., 2009). If IQ had been used as a covariant, the differences in cortical activation in ADHD and normal healthy control children would have been over-corrected since IQ is relevant to the brain phenotype of the disorder (de Zeeuw et al., 2012).

Moreover, IQ measurement of ADHD children poses a problem intrinsic to ADHD symptoms: it is sometimes difficult for young ADHD children to execute IQ tests as they are not always sufficiently patient. Thus, the IQs of ADHD children might be underestimated, and not adequately reliable.

Previous reports adopting an IQ match between ADHD and normal healthy children enrolled ADHD children with relatively high IQs (Aron et al., 2003; Booth et al., 2005; Chabernaud et al., 2012; Durston et al., 2007; Ma et al., 2012; Negoro et al., 2010; Schecklmann et al., 2010; Vaidya et al., 1998; Yerys et al., 2009). Most of these studies excluded low-IQ ADHD children with criteria such as IQ > 85 or IQ > 90 (Aron et al., 2003; Ma et al., 2012; Vaidya et al., 1998; Yerys et al., 2009). We calculated the average IQ of ADHD children in these studies and found that it was 108 ± 8 (mean $\pm$ SD). There is a possibility that low-IQ ADHD children with severe behavioral rating scores had been selectively excluded.

On the other hand, our IQ criterion was greater than 70, which is among the most lenient criterions together with two other recent studies (Inoue et al., 2012; Negoro et al., 2010). Such samples are expected to represent the ADHD population in a balanced manner as they include severe patients. While there might be other possibilities for matching ADHD IQs with those of normal healthy children with low IQs, it is difficult to match the IQs of normal healthy children to those of ADHD groups including children with low IQs, and no study has performed matching for such low scores. Moreover, even if IQ matching had been realized, such samples would not have represented general healthy children.

Although IQ matching for ADHD and control children poses several problems as mentioned above, we do not mean that it should be avoided. Rather, IQ-matching studies should be pursued with different perspectives, such as to assess the effects of IQ, and should be undertaken in the future. As de Zeeuw reported (de Zeeuw et al., 2012), the brains of low-IQ ADHD children might undergo different functional and anatomical development. If this is the case, subdividing the whole group to yield low-IQ groups would be of great clinical importance. For this purpose, the current system, which can measure severely ADHD children with low IQs, would serve as a valuable tool.

4.4. Limitations

A few limitations should be noted for adequate understanding of the current findings. First, a learning effect associated with go/no-go tasks cannot be excluded from the current experimental design: while control subjects underwent only one task session, ADHD children underwent two sessions in the same day. Thus, the effects of habituation (Fischer et al., 2003; Kiehl and Liddle, 2003; Loubinoux et al., 2001) and procedural learning (Eliassen et al., 2001) could be present. First-day pre-medicated data (i.e., either pre-placebo or pre-MPH) was used for the ADHD group to compare the two groups (ADHD and control) under conditions not affected by these factors. However, post-medication data are by necessity from the second sessions. For separate sessions of the same task, an activation of greater magnitude has been observed for the first session for go/no-go tasks in fMRI studies (Langenecker and Nielson, 2003). Thus, it was expected that the oxy-Hb amplitude of the second, post-medicated, sessions would be reduced. However, in the current study, MPH administration to ADHD children still led to increased oxy-Hb amplitude comparable to that of control children. This indicates that MPH exerted pharmacological effects beyond the level needed to compensate for the expected habituation and learning effects.

Second, the current study limited the analyses to the oxy-Hb parameter because we did not find any channels with significant activation with the deoxy-Hb parameter during the screening process performed on normal healthy control subjects. Thus, we concluded that deoxy-Hb was not suitable for further analysis in the current study.

Many fNIRS studies have solely reported the results of the oxy-Hb parameter, including an ADHD study by Negoro et al. (2010). There is a tendency that oxy-Hb is more sensitive than deoxy-Hb (e.g. Ehlis et al., 2008; Inoue et al., 2012; Weber et al., 2005), but the precise reason for the decreased sensitivity of deoxy-Hb has yet to be elucidated. Our previous study adopting a similar experimental paradigm also failed to detect activation with the deoxy-Hb parameter (Monden et al., 2012). Ehlis et al. (2008) reported that deoxy-Hb behavior was different between ADHD and normal subjects: deoxy-Hb decreases were larger in ADHD subjects than in normal subjects. In addition, even when oxy-Hb increased, the deoxy-Hb parameter either increased, remained unchanged or decreased depending on tasks, regions, age and so on (Ehlis et al., 2008; Sakatani et al., 1999), suggesting difficulty in dealing with the deoxy-Hb parameter. Further exploration is necessary to elucidate the role and applicability of the deoxy-Hb parameter.

4.5. Clinical utility of fNIRS-based examination

In the current study, we adopted a go/no-go task paradigm with alternating go and go/no-go blocks. Tsujii et al. (2011) and Cui et al. (2011) employed alternating go and go/no-go tasks, and used the go task as a baseline contrast for the go/no-go task fNIRS signal that they were interested in. Similarly, we used the go block as a baseline period, and did not adopt rest periods. This was primarily because it is extremely difficult for ADHD patients to stay still without performing any task: it may lead to unexpected movements or behaviors. Secondarily, we could save time by omitting rest blocks: a prolonged experiment time may bore ADHD subjects. Finally, experimental paradigms employing alternate go and go/no-go blocks have been commonly used in fMRI studies (Altshuler et al., 2005; Dillo et al., 2010; Ma et al., 2012; Vaidya et al., 1998) and also in fNIRS studies (Tsujii et al., 2011). Thus, considering comparisons across modalities, the choice of experimental paradigm in the current study is appropriate.

An additional merit of the alternative task paradigm is that go blocks can serve as a motor control for go/no-go blocks. Schecklmann et al. (2008) performed weekday reciting task and word fluency tasks and used the weekday reciting task as a baseline to which fNIRS signal during the word fluency tasks was compared. By using a control condition with a similar motor output, movement and muscle artifacts in a task condition are expected to be cancelled. Similarly, we adopted the go task as a baseline period. During the go task period, subjects are expected to press a button twice as often as in the go/no-go task period,

assuming that they perform the tasks appropriately. Due to the nature of go/no-go tasks, that go periods require increased response, we cannot fully equalize the motor loads of go and go/no-go periods. However, since motor effects are considered larger during the go period, we can expect that a go/no-go vs. go contrast would rule out motion artifacts. Accordingly, activation in a go/no-go task block is considered to reflect response inhibition and target detection, and is therefore more appropriate than a rest block as a baseline. Although fNIRS studies often use a paradigm where rest and task blocks were alternately performed (Herrmann et al., 2005), we suggest that it would be more suitable for studies using younger ADHD children to adopt experimental paradigms employing alternate go and go/no-go blocks, which have been commonly used in fMRI studies (Altshuler et al., 2005; Dillo et al., 2010; Ma et al., 2012; Vaidya et al., 1998).

5. Conclusion

In the current study exploring fNIRS-based diagnosis on the effects of MPH administration to ADHD children using a double-blind, placebo-controlled, cross-over design, we presented the following findings: 1) Relative to control subjects, unmedicated ADHD children exhibited reduced brain activation in the right IFG and MFG during go/no-go task blocks. 2) The reduced activation in the right inferior and middle frontal gyri was acutely normalized after MPH administration, but not after placebo administration. 3) Compared to the placebo-induced activation, the MPH-induced right IFG/MFG activation was significantly larger. These findings led us to conclude that the activation in the right inferior and middle frontal gyri could serve as an objective neuro-functional biomarker to indicate the effects of MPH on ADHD children. fNIRS-based examination on the effect of MPH was applicable to ADHD children as young as 6 years old. This promising technique will enable the early clinical diagnosis and treatment of ADHD children.

Acknowledgements

We appreciate ELCS for the English proofreading. We thank Illpop (http://illpop.com/animal_top01.htm) for kindly providing source pictures for the experimental materials. This work was supported in part by the Grant-in-Aid for Scientific Research from the Japan Society for Promotion of Science (22242012 to ID, 23390354 to EW, 23700885 to HD, 23650217 to ID, 80382951 to YM, and 70438662 to MN), and Health and Labor Sciences Research Grants, Research on Psychiatric and Neurological Diseases and Mental Health (to ID).

Appendix A. Supplementary data

Supplementary data to this article can be found online at http://dx.doi.org/10.1016/j.nicl.2012.10.001.

References

Altshuler, L.L., Bookheimer, S.Y., Townsend, J., Proenza, M.A., Eisenberger, N., Sabb, F., Mintz, J., Cohen, M.S., 2005. Blunted activation in orbitofrontal cortex during mania: a functional magnetic resonance imaging study. Biological Psychiatry 58, 763–769.

American Psychiatric Association, 1994. Diagnostic and Statistical Manual of Mental Disorders, 4th ed. American Psychiatric Association, Washington, DC.

Anderson, C.M., Polcari, A., Lowen, S.B., Renshaw, P.F., Teicher, M.H., 2002. Effects of methylphenidate on functional magnetic resonance relaxometry of the cerebellar vermis in boys with ADHD. The American Journal of Psychiatry 159, 1322–1328.

Arnsten, A.F., 2006. Stimulants: therapeutic actions in ADHD. Neuropsychopharmacology 31, 2376–2383.

Aron, A.R., Poldrack, R.A., 2005. The cognitive neuroscience of response inhibition: relevance for genetic research in attention-deficit/hyperactivity disorder. Biological Psychiatry 57, 1285–1292.

Aron, A.R., Dowson, J.H., Sahakian, B.J., Robbins, T.W., 2003. Methylphenidate improves response inhibition in adults with attention-deficit/hyperactivity disorder. Biological Psychiatry 54, 1465–1468.

Barkley, R.A., 1991. The ecological validity of laboratory and analogue assessment methods of ADHD symptoms. Journal of Abnormal Child Psychology 19, 149–178.

Beauregard, M., Levesque, J., 2006. Functional magnetic resonance imaging investigation of the effects of neurofeedback training on the neural bases of selective attention and response inhibition in children with attention-deficit/hyperactivity disorder. Applied Psychophysiology and Biofeedback 31, 3–20.

Bedard, A.C., Ickowicz, A., Logan, G.D., Hogg-Johnson, S., Schachar, R., Tannock, R., 2003. Selective inhibition in children with attention-deficit hyperactivity disorder off and on stimulant medication. Journal of Abnormal Child Psychology 31, 315–327.

Bedard, A.C., Schulz, K.P., Cook Jr., E.H., Fan, J., Clerkin, S.M., Ivanov, I., Halperin, J.M., Newcorn, J.H., 2010. Dopamine transporter gene variation modulates activation of striatum in youth with ADHD. NeuroImage 53, 935–942.

Biederman, J., Monuteaux, M.C., Spencer, T., Wilens, T.E., Faraone, S.V., 2009. Do stimulants protect against psychiatric disorders in youth with ADHD? A 10-year follow-up study. Pediatrics 124, 71–78.

Boecker, M., Buecheler, M.M., Schroeter, M.L., Gauggel, S., 2007. Prefrontal brain activation during stop-signal response inhibition: an event-related functional near-infrared spectroscopy study. Behavioural Brain Research 176, 259–266.

Booth, J.R., Burman, D.D., Meyer, J.R., Lei, Z., Trommer, B.L., Davenport, N.D., Li, W., Parrish, T.B., Gitelman, D.R., Mesulam, M.M., 2005. Larger deficits in brain networks for response inhibition than for visual selective attention in attention deficit hyperactivity disorder (ADHD). Journal of Child Psychology and Psychiatry 46, 94–111.

Buchsbaum, B.R., Greer, S., Chang, W.L., Berman, K.F., 2005. Meta-analysis of neuroimaging studies of the Wisconsin card-sorting task and component processes. Human Brain Mapping 25, 35–45.

Chabernaud, C., Mennes, M., Kelly, C., Nooner, K., Di Martino, A., Castellanos, F.X., Milham, M.P., 2012. Dimensional brain–behavior relationships in children with attention-deficit/hyperactivity disorder. Biological Psychiatry 71, 434–442.

Cope, M., Delpy, D.T., Reynolds, E.O., Wray, S., Wyatt, J., van der Zee, P., 1988. Methods of quantitating cerebral near infrared spectroscopy data. Advances in Experimental Medicine and Biology 222, 183–189.

Cui, X., Bray, S., Bryant, D.M., Glover, G.H., Reiss, A.L., 2011. A quantitative comparison of NIRS and fMRI across multiple cognitive tasks. NeuroImage 54, 2808–2821.

de Zeeuw, P., Schnack, H.G., van Belle, J., Weusten, J., van Dijk, S., Langen, M., Brouwer, R.M., van Engeland, H., Durston, S., 2012. Differential brain development with low and high IQ in attention-deficit/hyperactivity disorder. PLoS One 7, e35770.

Dennis, M., Francis, D.J., Cirino, P.T., Schachar, R., Barnes, M.A., Fletcher, J.M., 2009. Why IQ is not a covariate in cognitive studies of neurodevelopmental disorders. Journal of the International Neuropsychological Society 15, 331–343.

Derefinko, K.J., Adams, Z.W., Milich, R., Fillmore, M.T., Lorch, E.P., Lynam, D.R., 2008. Response style differences in the inattentive and combined subtypes of attention-deficit/hyperactivity disorder. Journal of Abnormal Child Psychology 36, 745–758.

Dibbets, P., Evers, L., Hurks, P., Marchetta, N., Jolles, J., 2009. Differences in feedback- and inhibition-related neural activity in adult ADHD. Brain and Cognition 70, 73–83.

Dillo, W., Goke, A., Prox-Vagedes, V., Szycik, G.R., Roy, M., Donnerstag, F., Emrich, H.M., Ohlmeier, M.D., 2010. Neuronal correlates of ADHD in adults with evidence for compensation strategies—a functional MRI study with a Go/No-Go paradigm. German Medical Science 8, Doc09.

Dittmann, R.W., Wehmeier, P.M., Schacht, A., Minarzyk, A., Lehmann, M., Sevecke, K., Lehmkuhl, G., 2009. Atomoxetine treatment and ADHD-related difficulties as assessed by adolescent patients, their parents and physicians. Child and Adolescent Psychiatry and Mental Health 3, 21.

Drechsler, R., Brandeis, D., Foldenyi, M., Imhof, K., Steinhausen, H.C., 2005. The course of neuropsychological functions in children with attention deficit hyperactivity disorder from late childhood to early adolescence. Journal of Child Psychology and Psychiatry 46, 824–836.

Durston, S., Thomas, K.M., Worden, M.S., Yang, Y., Casey, B.J., 2002. The effect of preceding context on inhibition: an event-related fMRI study. NeuroImage 16, 449–453.

Durston, S., Tottenham, N.T., Thomas, K.M., Davidson, M.C., Eigsti, I.M., Yang, Y., Ulug, A.M., Casey, B.J., 2003. Differential patterns of striatal activation in young children with and without ADHD. Biological Psychiatry 53, 871–878.

Durston, S., Hulshoff Pol, H.E., Schnack, H.G., Buitelaar, J.K., Steenhuis, M.P., Minderaa, R.B., Kahn, R.S., van Engeland, H., 2004. Magnetic resonance imaging of boys with attention-deficit/hyperactivity disorder and their unaffected siblings. Journal of the American Academy of Child and Adolescent Psychiatry 43, 332–340.

Durston, S., Davidson, M.C., Mulder, M.J., Spicer, J.A., Galvan, A., Tottenham, N., Scheres, A., Xavier Castellanos, F., van Engeland, H., Casey, B.J., 2007. Neural and behavioral correlates of expectancy violations in attention-deficit hyperactivity disorder. Journal of Child Psychology and Psychiatry 48, 881–889.

Ehlis, A.C., Bahne, C.G., Jacob, C.P., Herrmann, M.J., Fallgatter, A.J., 2008. Reduced lateral prefrontal activation in adult patients with attention-deficit/hyperactivity disorder (ADHD) during a working memory task: a functional near-infrared spectroscopy (fNIRS) study. Journal of Psychiatric Research 42, 1060–1067.

Eliassen, J.C., Souza, T., Sanes, J.N., 2001. Human brain activation accompanying explicitly directed movement sequence learning. Experimental Brain Research 141, 269–280.

Epstein, J.N., Casey, B.J., Tonev, S.T., Davidson, M., Reiss, A.L., Garrett, A., Hinshaw, S.P., Greenhill, L.L., Vitolo, A., Kotler, L.A., Jarrett, M.A., Spicer, J., 2007. Assessment and prevention of head motion during imaging of patients with attention deficit hyperactivity disorder. Psychiatry Research 155, 75–82.

Fair, D.A., Posner, J., Nagel, B.J., Bathula, D., Dias, T.G., Mills, K.L., Blythe, M.S., Giwa, A., Schmitt, C.F., Nigg, J.T., 2010. Atypical default network connectivity in youth with attention-deficit/hyperactivity disorder. Biological Psychiatry 68, 1084–1091.

Fischer, H., Wright, C.I., Whalen, P.J., McInerney, S.C., Shin, L.M., Rauch, S.L., 2003. Brain habituation during repeated exposure to fearful and neutral faces: a functional MRI study. Brain Research Bulletin 59, 387–392.

Frazier, T.W., Demaree, H.A., Youngstrom, E.A., 2004. Meta-analysis of intellectual and neuropsychological test performance in attention-deficit/hyperactivity disorder. Neuropsychology 18, 543–555.
Garavan, H., Ross, T.J., Stein, E.A., 1999. Right hemispheric dominance of inhibitory control: an event-related functional MRI study. Proceedings of the National Academy of Sciences of the United States of America 96, 8301–8306.
Garavan, H., Ross, T.J., Murphy, K., Roche, R.A., Stein, E.A., 2002. Dissociable executive functions in the dynamic control of behavior: inhibition, error detection, and correction. NeuroImage 17, 1820–1829.
Garavan, H., Ross, T.J., Kaufman, J., Stein, E.A., 2003. A midline dissociation between error-processing and response-conflict monitoring. NeuroImage 20, 1132–1139.
Garavan, H., Hester, R., Murphy, K., Fassbender, C., Kelly, C., 2006. Individual differences in the functional neuroanatomy of inhibitory control. Brain Research 1105, 130–142.
Grafton, S.T., Mazziotta, J.C., Woods, R.P., Phelps, M.E., 1992. Human functional anatomy of visually guided finger movements. Brain 115 (Pt 2), 565–587.
Herrmann, M.J., Ehlis, A.C., Fallgatter, A.J., 2004. Bilaterally reduced frontal activation during a verbal fluency task in depressed patients as measured by near-infrared spectroscopy. The Journal of Neuropsychiatry and Clinical Neurosciences 16, 170–175.
Herrmann, M.J., Plichta, M.M., Ehlis, A.C., Fallgatter, A.J., 2005. Optical topography during a Go–NoGo task assessed with multi-channel near-infrared spectroscopy. Behavioural Brain Research 160, 135–140.
Hester, R.L., Murphy, K., Foxe, J.J., Foxe, D.M., Javitt, D.C., Garavan, H., 2004. Predicting success: patterns of cortical activation and deactivation prior to response inhibition. Journal of Cognitive Neuroscience 16, 776–785.
Hock, C., Villringer, K., Müller-Spahn, F., Wenzel, R., Heekeren, H., Schuh-Hofer, S., Hofmann, M., Minoshima, S., Schwaiger, M., Dirnagl, U., Villringer, A., 1997. Decrease in parietal cerebral hemoglobin oxygenation during performance of a verbal fluency task in patients with Alzheimer's disease monitored by means of near-infrared spectroscopy (NIRS) — correlation with simultaneous rCBF-PET measurements. Brain Research 755, 293–303.
Inoue, Y., Sakihara, K., Gunji, A., Ozawa, H., Kimiya, S., Shinoda, H., Kaga, M., Inagaki, M., 2012. Reduced prefrontal hemodynamic response in children with ADHD during the go/nogo task: a NIRS study. Neuroreport 23, 55–60.
Jourdan Moser, S., Cutini, S., Weber, P., Schroeter, M.L., 2009. Right prefrontal brain activation due to Stroop interference is altered in attention-deficit hyperactivity disorder — a functional near-infrared spectroscopy study. Psychiatry Research 173, 190–195.
Jurcak, V., Tsuzuki, D., Dan, I., 2007. 10/20, 10/10, and 10/5 systems revisited: their validity as relative head-surface-based positioning systems. NeuroImage 34, 1600–1611.
Karch, S., Thalmeier, T., Lutz, J., Cerovecki, A., Opgen-Rhein, M., Hock, B., Leicht, G., Hennig-Fast, K., Meindl, T., Riedel, M., Mulert, C., Pogarell, O., 2010. Neural correlates (ERP/fMRI) of voluntary selection in adult ADHD patients. European Archives of Psychiatry and Clinical Neuroscience 260, 427–440.
Kiehl, K.A., Liddle, P.F., 2003. Reproducibility of the hemodynamic response to auditory oddball stimuli: a six-week test–retest study. Human Brain Mapping 18, 42–52.
Konishi, S., Nakajima, K., Uchida, I., Kikyo, H., Kameyama, M., Miyashita, Y., 1999. Common inhibitory mechanism in human inferior prefrontal cortex revealed by event-related functional MRI. Brain 122 (Pt 5), 981–991.
Kuntsi, J., Eley, T.C., Taylor, A., Hughes, C., Asherson, P., Caspi, A., Moffitt, T.E., 2004. Co-occurrence of ADHD and low IQ has genetic origins. American Journal of Medical Genetics. Part B, Neuropsychiatric Genetics 124B, 41–47.
Langenecker, S.A., Nielson, K.A., 2003. Frontal recruitment during response inhibition in older adults replicated with fMRI. NeuroImage 20, 1384–1392.
Law, I., Svarer, C., Holm, S., Paulson, O.B., 1997. The activation pattern in normal humans during suppression, imagination and performance of saccadic eye movements. Acta Physiologica Scandinavica 161, 419–434.
Liddle, P.F., Kiehl, K.A., Smith, A.M., 2001. Event-related fMRI study of response inhibition. Human Brain Mapping 12, 100–109.
Loubinoux, I., Carel, C., Alary, F., Boulanouar, K., Viallard, G., Manelfe, C., Rascol, O., Celsis, P., Chollet, F., 2001. Within-session and between-session reproducibility of cerebral sensorimotor activation: a test–retest effect evidenced with functional magnetic resonance imaging. Journal of Cerebral Blood Flow and Metabolism 21, 592–607.
Ma, J., Lei, D., Jin, X., Du, X., Jiang, F., Li, F., Zhang, Y., Shen, X., 2012. Compensatory brain activation in children with attention deficit/hyperactivity disorder during a simplified go/no-go task. Journal of Neural Transmission 119, 613–619.
Maki, A., Yamashita, Y., Ito, Y., Watanabe, E., Mayanagi, Y., Koizumi, H., 1995. Spatial and temporal analysis of human motor activity using noninvasive NIR topography. Medical Physics 22, 1997–2005.
Matsuo, K., Kato, T., Fukuda, M., Kato, N., 2000. Alteration of hemoglobin oxygenation in the frontal region in elderly depressed patients as measured by near-infrared spectroscopy. The Journal of Neuropsychiatry and Clinical Neurosciences 12, 465–471.
Matsuo, K., Taneichi, K., Matsumoto, A., Ohtani, T., Yamasue, H., Sakano, Y., Sasaki, T., Sadamatsu, M., Kasai, K., Iwanami, A., Asukai, N., Kato, N., Kato, T., 2003. Hypoactivation of the prefrontal cortex during verbal fluency test in PTSD: a near-infrared spectroscopy study. Psychiatry Research 124, 1–10.
Menon, V., Adleman, N.E., White, C.D., Glover, G.H., Reiss, A.L., 2001. Error-related brain activation during a go/nogo response inhibition task. Human Brain Mapping 12, 131–143.
Monden, Y., Dan, H., Nagashima, M., Dan, I., Kyutoku, Y., Okamoto, M., Yamagata, T., Momoi, M.Y., Watanabe, E., 2012. Clinically-oriented monitoring of acute effects of methylphenidate on cerebral hemodynamics in ADHD children using fNIRS. Clinical Neurophysiology 123, 1147–1157.
Moriai-Izawa, A., Dan, H., Dan, I., Sano, T., Oguro, K., Yokota, H., Tsuzuki, D., Watanabe, E., 2012. Multichannel fNIRS assessment of overt and covert confrontation naming. Brain and Language 121, 185–193.
Mostofsky, S.H., Simmonds, D.J., 2008. Response inhibition and response selection: two sides of the same coin. Journal of Cognitive Neuroscience 20, 751–761.
Mostofsky, S.H., Schafer, J.G., Abrams, M.T., Goldberg, M.C., Flower, A.A., Boyce, A., Courtney, S.M., Calhoun, V.D., Kraut, M.A., Denckla, M.B., Pekar, J.J., 2003. fMRI evidence that the neural basis of response inhibition is task-dependent. Brain Research. Cognitive Brain Research 17, 419–430.
Mulligan, R.C., Knopik, V.S., Sweet, L.H., Fischer, M., Seidenberg, M., Rao, S.M., 2011. Neural correlates of inhibitory control in adult attention deficit/hyperactivity disorder: evidence from the Milwaukee longitudinal sample. Psychiatry Research 194, 119–129.
Negoro, H., Sawada, M., Iida, J., Ota, T., Tanaka, S., Kishimoto, T., 2010. Prefrontal dysfunction in attention-deficit/hyperactivity disorder as measured by near-infrared spectroscopy. Child Psychiatry and Human Development 41, 193–203.
Newcorn, J.H., Halperin, J.M., Jensen, P.S., Abikoff, H.B., Arnold, L.E., Cantwell, D.P., Conners, C.K., Elliott, G.R., Epstein, J.N., Greenhill, L.L., Hechtman, L., Hinshaw, S.P., Hoza, B., Kraemer, H.C., Pelham, W.E., Severe, J.B., Swanson, J.M., Wells, K.C., Wigal, T., Vitiello, B., 2001. Symptom profiles in children with ADHD: effects of comorbidity and gender. Journal of the American Academy of Child and Adolescent Psychiatry 40, 137–146.
Okamoto, M., Dan, I., 2005. Automated cortical projection of head-surface locations for transcranial functional brain mapping. NeuroImage 26, 18–28.
Okamoto, M., Dan, H., Sakamoto, K., Takeo, K., Shimizu, K., Kohno, S., Oda, I., Isobe, S., Suzuki, T., Kohyama, K., Dan, I., 2004a. Three-dimensional probabilistic anatomical cranio-cerebral correlation via the international 10–20 system oriented for transcranial functional brain mapping. NeuroImage 21, 99–111.
Okamoto, M., Dan, H., Shimizu, K., Takeo, K., Amita, T., Oda, I., Konishi, I., Sakamoto, K., Isobe, S., Suzuki, T., Kohyama, K., Dan, I., 2004b. Multimodal assessment of cortical activation during apple peeling by NIRS and fMRI. NeuroImage 21, 1275–1288.
Okamoto, M., Matsunami, M., Dan, H., Kohata, T., Kohyama, K., Dan, I., 2006. Prefrontal activity during taste encoding: an fNIRS study. NeuroImage 31, 796–806.
Peterson, B.S., Potenza, M.N., Wang, Z., Zhu, H., Martin, A., Marsh, R., Plessen, K.J., Yu, S., 2009. An FMRI study of the effects of psychostimulants on default-mode processing during Stroop task performance in youths with ADHD. The American Journal of Psychiatry 166, 1286–1294.
Pietrzak, R.H., Mollica, C.M., Maruff, P., Snyder, P.J., 2006. Cognitive effects of immediate-release methylphenidate in children with attention-deficit/hyperactivity disorder. Neuroscience and Biobehavioral Reviews 30, 1225–1245.
Rorden, C., Brett, M., 2000. Stereotaxic display of brain lesions. Behavioural Neurology 12, 191–200.
Rubia, K., Overmeyer, S., Taylor, E., Brammer, M., Williams, S.C., Simmons, A., Bullmore, E.T., 1999. Hypofrontality in attention deficit hyperactivity disorder during higher-order motor control: a study with functional MRI. The American Journal of Psychiatry 156, 891–896.
Rubia, K., Russell, T., Overmeyer, S., Brammer, M.J., Bullmore, E.T., Sharma, T., Simmons, A., Williams, S.C., Giampietro, V., Andrew, C.M., Taylor, E., 2001. Mapping motor inhibition: conjunctive brain activations across different versions of go/no-go and stop tasks. NeuroImage 13, 250–261.
Rubia, K., Smith, A.B., Brammer, M.J., Taylor, E., 2003. Right inferior prefrontal cortex mediates response inhibition while mesial prefrontal cortex is responsible for error detection. NeuroImage 20, 351–358.
Rubia, K., Smith, A.B., Brammer, M.J., Toone, B., Taylor, E., 2005. Abnormal brain activation during inhibition and error detection in medication-naive adolescents with ADHD. The American Journal of Psychiatry 162, 1067–1075.
Rubia, K., Halari, R., Cubillo, A., Mohammad, A.M., Brammer, M., Taylor, E., 2009. Methylphenidate normalises activation and functional connectivity deficits in attention and motivation networks in medication-naive children with ADHD during a rewarded continuous performance task. Neuropharmacology 57, 640–652.
Sakatani, K., Lichty, W., Xie, Y., Li, S., Zuo, H., 1999. Effects of aging on language-activated cerebral blood oxygenation changes of the left prefrontal cortex: Near infrared spectroscopy study. Journal of Stroke and Cerebrovascular Diseases 8, 398–403.
Schecklmann, M., Ehlis, A.C., Plichta, M.M., Romanos, J., Heine, M., Boreatti-Hummer, A., Jacob, C., Fallgatter, A.J., 2008. Diminished prefrontal oxygenation with normal and above-average verbal fluency performance in adult ADHD. Journal of Psychiatric Research 43, 98–106.
Schecklmann, M., Romanos, M., Bretscher, F., Plichta, M.M., Warnke, A., Fallgatter, A.J., 2010. Prefrontal oxygenation during working memory in ADHD. Journal of Psychiatric Research 44, 621–628.
Schulz, K.P., Fan, J., Tang, C.Y., Newcorn, J.H., Buchsbaum, M.S., Cheung, A.M., Halperin, J.M., 2004. Response inhibition in adolescents diagnosed with attention deficit hyperactivity disorder during childhood: an event-related FMRI study. The American Journal of Psychiatry 161, 1650–1657.
Sebastian, A., Gerdes, B., Feige, B., Kloppel, S., Lange, T., Philipsen, A., Tebartz van Elst, L., Lieb, K., Tuscher, O., 2012. Neural correlates of interference inhibition, action withholding and action cancelation in adult ADHD. Psychiatry Research 202, 132–141.
Shattuck, D.W., Mirza, M., Adisetiyo, V., Hojatkashani, C., Salamon, G., Narr, K.L., Poldrack, R.A., Bilder, R.M., Toga, A.W., 2008. Construction of a 3D probabilistic atlas of human cortical structures. NeuroImage 39, 1064–1080.
Shinba, T., Nagano, M., Kariya, N., Ogawa, K., Shinozaki, T., Shimosato, S., Hoshi, Y., 2004. Near-infrared spectroscopy analysis of frontal lobe dysfunction in schizophrenia. Biological Psychiatry 55, 154–164.
Simmonds, D.J., Pekar, J.J., Mostofsky, S.H., 2008. Meta-analysis of go/no-go tasks demonstrating that fMRI activation associated with response inhibition is task-dependent. Neuropsychologia 46, 224–232.

Singh, A.K., Okamoto, M., Dan, H., Jurcak, V., Dan, I., 2005. Spatial registration of multichannel multi-subject fNIRS data to MNI space without MRI. NeuroImage 27, 842–851.
Siniatchkin, M., Glatthaar, N., von Muller, G.G., Prehn-Kristensen, A., Wolff, S., Knochel, S., Steinmann, E., Sotnikova, A., Stephani, U., Petermann, F., Gerber, W.D., 2012. Behavioural treatment increases activity in the cognitive neuronal networks in children with attention deficit/hyperactivity disorder. Brain Topography 25, 332–344.
Slifer, K.J., Koontz, K.L., Cataldo, M.F., 2002. Operant-contingency-based preparation of children for functional magnetic resonance imaging. Journal of Applied Behavior Analysis 35, 191–194.
Smith, A.B., Taylor, E., Brammer, M., Toone, B., Rubia, K., 2006. Task-specific hypoactivation in prefrontal and temporoparietal brain regions during motor inhibition and task switching in medication-naive children and adolescents with attention deficit hyperactivity disorder. The American Journal of Psychiatry 163, 1044–1051.
Solanto, M.V., Schulz, K.P., Fan, J., Tang, C.Y., Newcorn, J.H., 2009. Event-related FMRI of inhibitory control in the predominantly inattentive and combined subtypes of ADHD. Journal of Neuroimaging 19, 205–212.
Spencer, T.J., 2004. ADHD treatment across the life cycle. The Journal of Clinical Psychiatry 65 (Suppl. 3), 22–26.
Strangman, G., Boas, D.A., Sutton, J.P., 2002. Non-invasive neuroimaging using near-infrared light. Biological Psychiatry 52, 679–693.
Suto, T., Fukuda, M., Ito, M., Uehara, T., Mikuni, M., 2004. Multichannel near-infrared spectroscopy in depression and schizophrenia: cognitive brain activation study. Biological Psychiatry 55, 501–511.
Tamm, L., Menon, V., Ringel, J., Reiss, A.L., 2004. Event-related fMRI evidence of frontotemporal involvement in aberrant response inhibition and task switching in attention-deficit/hyperactivity disorder. Journal of the American Academy of Child and Adolescent Psychiatry 43, 1430–1440.
Tannock, R., Schachar, R., Logan, G., 1995. Methylphenidate and cognitive flexibility: dissociated dose effects in hyperactive children. Journal of Abnormal Child Psychology 23, 235–266.
Teicher, M.H., Anderson, C.M., Polcari, A., Glod, C.A., Maas, L.C., Renshaw, P.F., 2000. Functional deficits in basal ganglia of children with attention-deficit/hyperactivity disorder shown with functional magnetic resonance imaging relaxometry. Nature Medicine 6, 470–473.
Tsujii, T., Sakatani, K., Nakashima, E., Igarashi, T., Katayama, Y., 2011. Characterization of the acute effects of alcohol on asymmetry of inferior frontal cortex activity during a go/no-go task using functional near-infrared spectroscopy. Psychopharmacology 217, 595–603.
Tsuzuki, D., Jurcak, V., Singh, A.K., Okamoto, M., Watanabe, E., Dan, I., 2007. Virtual spatial registration of stand-alone fNIRS data to MNI space. NeuroImage 34, 1506–1518.
Tsuzuki, D., Cai, D.S., Dan, H., Kyutoku, Y., Fujita, A., Watanabe, E., Dan, I., 2012. Stable and convenient spatial registration of stand-alone NIRS data through anchor-based probabilistic registration. Neuroscience Research 72, 163–171.
Vaidya, C.J., Austin, G., Kirkorian, G., Ridlehuber, H.W., Desmond, J.E., Glover, G.H., Gabrieli, J.D., 1998. Selective effects of methylphenidate in attention deficit hyperactivity disorder: a functional magnetic resonance study. Proceedings of the National Academy of Sciences of the United States of America 95, 14494–14499.
Vaidya, C.J., Bunge, S.A., Dudukovic, N.M., Zalecki, C.A., Elliott, G.R., Gabrieli, J.D., 2005. Altered neural substrates of cognitive control in childhood ADHD: evidence from functional magnetic resonance imaging. The American Journal of Psychiatry 162, 1605–1613.
Vasic, N., Plichta, M.M., Wolf, R.C., Fallgatter, A.J., Sosic-Vasic, Z., Gron, G., in press. Reduced neural error signaling in left inferior prefrontal cortex in young adults with ADHD. Journal of Attention Disorders.
Weber, P., Lutschg, J., Fahnenstich, H., 2005. Cerebral hemodynamic changes in response to an executive function task in children with attention-deficit hyperactivity disorder measured by near-infrared spectroscopy. Journal of Developmental and Behavioral Pediatrics 26, 105–111.
Wehmeier, P.M., Schacht, A., Wolff, C., Otto, W.R., Dittmann, R.W., Banaschewski, T., 2011. Neuropsychological outcomes across the day in children with attention-deficit/hyperactivity disorder treated with atomoxetine: results from a placebo-controlled study using a computer-based continuous performance test combined with an infra-red motion-tracking device. Journal of Child and Adolescent Psychopharmacology 21, 433–444.
Wilens, T.E., 2008. Effects of methylphenidate on the catecholaminergic system in attention-deficit/hyperactivity disorder. Journal of Clinical Psychopharmacology 28, S46–S53.
Yerys, B.E., Jankowski, K.F., Shook, D., Rosenberger, L.R., Barnes, K.A., Berl, M.M., Ritzl, E.K., Vanmeter, J., Vaidya, C.J., Gaillard, W.D., 2009. The fMRI success rate of children and adolescents: typical development, epilepsy, attention deficit/hyperactivity disorder, and autism spectrum disorders. Human Brain Mapping 30, 3426–3435.
Zhu, C.Z., Zang, Y.F., Cao, Q.J., Yan, C.G., He, Y., Jiang, T.Z., Sui, M.Q., Wang, Y.F., 2008. Fisher discriminative analysis of resting-state brain function for attention-deficit/hyperactivity disorder. NeuroImage 40, 110–120.

NeuroImage 85 (2014) 92–103

Contents lists available at ScienceDirect

NeuroImage

journal homepage: www.elsevier.com/locate/ynimg

Review

Spatial registration for functional near-infrared spectroscopy: From channel position on the scalp to cortical location in individual and group analyses☆

Daisuke Tsuzuki *, Ippeita Dan *

Functional Brain Science Laboratory, Jichi Medical University, 3311-1 Yakushiji, Shimotsuke, Tochigi 329-0498, Japan
Applied Cognitive Neuroscience Laboratory, Research and Development Initiatives, Chuo University, 1-13-27 Kasuga, Bunkyo-ward, Tokyo 112-8551, Japan

ARTICLE INFO

Article history:
Accepted 4 July 2013
Available online 25 July 2013

Keywords:
Optical topography
International 10–20 system
Normalization
Talairach system
Stereotactic coordinate system
3D-digitizer

ABSTRACT

Functional near-infrared spectroscopy (fNIRS) has now become widely accepted as a common functional imaging modality. In order for fNIRS to achieve genuine neuroimaging citizenship, it would ideally be equipped with functional and structural image analyses. However, fNIRS measures cortical activities from the head surface without anatomical information of the object being measured. In this review article, we will present a methodological overview of spatial registration of fNIRS data to overcome this technical drawback of fNIRS. We first introduce and explore the use of standard stereotaxic space and anatomical labeling. Second, we explain different ways of describing scalp landmarks using 10–20 based systems. Third, we describe the simplest case of fNIRS data co-registration to a subject's own MRI. Fourth, we extend the concept to fNIRS data registration of group data. Fifth, we describe probabilistic registration methods, which use a reference-MRI database instead of a subject's own MRIs, and thus enable MRI-free registration for standalone fNIRS data. Sixth, we further extend the concept of probabilistic registration to three-dimensional image reconstruction in diffuse optical tomography. Seventh, we describe a 3D-digitizer-free method for the virtual registration of fNIRS data. Eighth, we provide practical guidance on how these techniques are implemented in software. Finally, we provide information on current resources and limitations for spatial registration of child and infant data. Through these technical descriptions, we stress the importance of presenting fNIRS data on a common platform to facilitate both intra- and inter-modal data sharing among the neuroimaging community.

Contents

* Corresponding authors at: Functional Brain Science Laboratory, Jichi Medical University, 3311-1 Yakushiji, Shimotsuke, Tochigi 329-0498, Japan.
E-mail addresses: tsuzukid@tamacc.chuo-u.ac.jp (D. Tsuzuki), dan@jichi.ac.jp (I. Dan).

1053-8119/$ – see front matter © 2013 The Authors. Published by Elsevier Inc. All rights reserved.
http://dx.doi.org/10.1016/j.neuroimage.2013.07.025

Introduction

Brain function and brain structure are intrinsically linked to each other. Whether one's interests lie in the function of a particular cortical region or functional network in a certain mental state, the function is described in reference to structure. Together, structural and functional images form the indispensable two wheels of human neuroimaging, and they should be linked through a process called registration (reviewed in Gholipour et al., 2007). While this is also applicable to functional near-infrared spectroscopy (fNIRS), fNIRS poses a distinct problem: the unavailability of structural information.

fNIRS typically measures relative hemoglobin signal changes to estimate cortical hemodynamics or the oxygenation state of cortical tissues, or sometimes cytochrome oxidase activity to estimate cortical metabolic state (reviewed in Obrig and Villringer, 2003). The basic concept of fNIRS for monitoring the hemodynamics of human tissue was first presented by Jobsis (1977). Later, the near-infrared technique was applied to measure hemodynamics associated with functional cortical activity in the early 1990s (Chance et al., 1993; Hoshi and Tamura, 1993; Kato et al., 1993; Villringer et al., 1993), representing the advent of fNIRS (reviewed in Ferrari and Quaresima, 2012).

In these early days, the number of source–detector probe pairs, or channels, was limited to one, or at most a few channels distantly placed to avoid light interference. Multichannel fNIRS instruments were then developed with an array of multiple source–detector pairs that allowed simultaneous monitoring across brain regions (Maki et al., 1995). Multichannel fNIRS data are often treated in a discrete manner, and subjected to channel-wise statistical analysis within a subject (e.g., Schroeter et al., 2002) or among a group of subjects (e.g., Okamoto et al., 2004b). To form spatially continuous functional images, these multichannel fNIRS data have been transformed via spatial interpolation to generate two-dimensional topographic images of brain activation (Maki et al., 1995). Moreover, when head and brain tissues are segmented, the light propagation from a source to a detector can be simulated (Okada et al., 1997). Accordingly, a continuous image is reconstructed to provide more accurate source estimations using short and long distance measurements to provide depth resolution. The resulting two- or three-dimensional reconstructed images are called diffuse optical imaging (DOI) or diffuse optical tomography (DOT) (Barbour et al., 1995; Bluestone et al., 2001; Boas et al., 2004; Culver et al., 2003; Note: DOI and DOT are usually used interchangeably with the latter favoring three-dimensional imaging).

However, fNIRS data is primarily obtained from the head surface without structural information for the brain. Thus, fNIRS measures brain activation, but cannot identify the source of activation on the cortical structure. In order to spatially assess fNIRS data, we must find the correspondence between the scalp location where an fNIRS measurement is performed, and its underlying cortical surface where the source signal is located. Namely, fNIRS data obtained on the scalp should be registered to its underlying cortical surface.

Hence, in this review article, we will present a methodological overview of spatial registration of fNIRS data. First we introduce and explore the use of standard stereotaxic space and anatomical labeling. Then we explain different ways of describing scalp landmarks using 10–20 based systems. Next, we describe the co-registration of fNIRS data to a subject's own MRI, and extend this to fNIRS data registration of group data. Combining these techniques, we describe probabilistic registration methods, which use a reference-MRI database instead of a subject's own MRIs thus enabling MRI-free registration. Subsequently, we extend the concept of probabilistic registration to three-dimensional (3D) image reconstruction in DOT. Moreover, we describe a 3D-digitizer-free method for the virtual registration of fNIRS data onto the stereotactic brain coordinate system. After presenting this theoretical framework, we provide practical guidance on how these techniques are implemented in software. To introduce an ongoing technical front, we also provide current resources and limitations for the spatial registration of child and infant data. Finally, we discuss the future direction of the spatial registration of fNIRS data.

Standard stereotaxic coordinate system

In group studies, functional data must be integrated across subjects to generate a unified inference. While a functional image can be obtained for individual inference, as for a case study or an individual diagnosis, in many cases inference is made for the population from which the subjects are extracted. However, as functional data are tightly bound to structure, integration should also be performed for structure. This is not a straightforward process, as cortical structures vary across subjects.

In considering fNIRS, let us assume a case where we have multichannel data co-registered to subjects' own MRIs. The problem is that structural MRIs have different shapes and sizes and that the orientations of sulci are as unique as fingerprints. One working solution, long sought by researchers, to cope with such structural variability is to standardize the brain structure to achieve a common anatomical platform (Brett et al., 2002). The first legendary achievement was Brodmann's atlas, in which Brodmann examined the cytochemical architecture of a cerebral cortex, and classified the cortex into approximately 50 different regions for humans (Brodmann, 1908). From the time of its invention, the two-dimensional sketch served as the standard for describing cortical anatomy for 80 years. Next came the advent of the Talairach atlas (Talairach and Tournoux, 1988), which is based on the intensively examined brain of a single subject: an elderly Caucasian woman. Two important features of the atlas are the introduction of the stereotactic coordinate system, which describes major anatomical structures of the brain in common three-dimensional space, and its inclusion of descriptions of all of the Brodmann regions. Even today, this atlas serves as a standard system, mostly because several popular analytical software packages for fMRI, including AFNI (Analysis of Functional Neuroimages), have adopted it as their standard coordinate system (Cox, 1996), with the original coordinates being modified to originate at the anterior commissure and the y axis to pass through the posterior commissure.

One major problem with the Talairach atlas is that it is based on a single subject's brain, and thus the shape and anatomical structures are biased. To compensate for this, an averaged brain template, made by co-registering different brains, is used as an alternative. The most widely used template, called MNI (Montreal Neurological Institute) 152 (also known as ICBM 152, where ICBM stands for International Consortium for Brain Mapping) was created by averaging 152 brains co-registered to the Talairach brain (Collins et al., 1994). MNI152 is a relatively unbiased representative of the gross human brain structure. It is widely used as a standard template for SPM (Statistical Parametric Mapping) (Friston et al., 1994). However, global standardization necessarily entails the loss of anatomical detail. Substantial averaging cancels out individual differences in cortical structures. Consequently, the MNI template has a smooth surface without sulci, except for some traces of Sylvian fissures, but it provides a common space for probabilistic description, thereby allowing us to statistically assess both functional activation and anatomical data (Fig. 1B). For example, specific functional activation data may be bound for a particular voxel [−62, 2, 31] and neighboring voxels, and anatomically this activation focus is most likely located on the left central gyrus. Such inference aiming at generalization is best made possible on an unbiased standard brain to represent the brain anatomy of the general population, rather than a canonical brain based on single subject's anatomy.

Anatomical information in MNI space is most conveniently achieved in reference to the Colin27 standard brain (Fig. 1A), which was made by averaging 27 scans of structural MRIs for an individual normalized to MNI space (Collins et al., 1994; Note: "Colin" is the subject and "Collins" is the author). One useful resource is the automatic anatomical labeling (AAL) tool originally provided as a toolbox for SPM (Tzourio-Mazoyer et al., 2002) (Figs. 1C and 2A, D). AAL presents a complete description

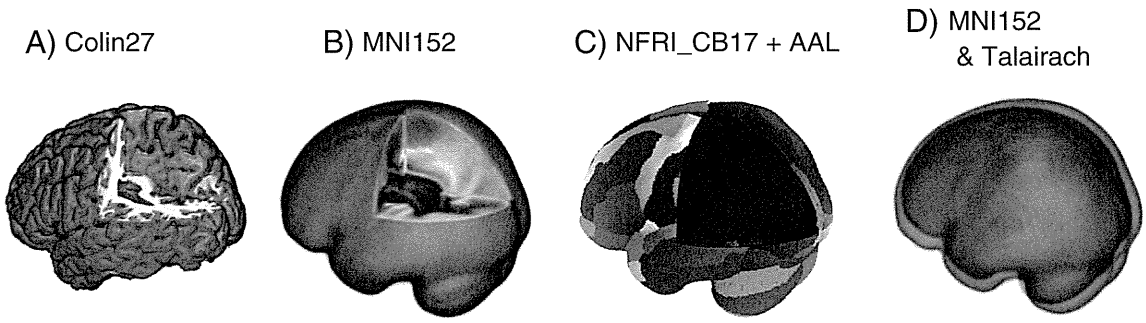

Fig. 1. Comparison among standard brains. All standard brains are aligned in and viewed from the same angle. (A) Colin27 with macro-anatomical information. (B) MNI152 template with smoothed cortical structures due to averaging. (C) NFRI_CB17 (National Food Research Institute Canonical Brain 17) optimized for fNIRS data registration. Cortical surface is compressed to a single layer to form a shell, where additional structural information such as macro-anatomical atlases and 10/20 landmarks may be registered. In this case, a mode-filtered AAL is overlaid. (D) MNI and Talairach templates aligned in the same coordinate system. Although they have similar shapes, the Talairach template is slightly smaller.

of the macro-anatomical structure of the Colin27 brain in terms of x, y, and z co-ordinates, called voxels, in MNI space. AAL returns estimate for a macro-anatomical structure for given MNI coordinates. If the given co-ordinate is located in areas A, B, and/or C, the AAL tool will produce a list of these areas along with their anatomical labels (Label A, Label B, Label C). A similar resource, called Talairach Daemon, is also available for the Talairach coordinate system (Lancaster et al., 2000). It should be noted here that MNI and Talairach space can be confused with one another; but, while they are similar, they are indeed different (Fig. 1D). Conversion between MNI and Talairach spaces are made in a convenient Matlab toolbox, icbm2tal (Laird et al., 2010; Lancaster et al., 2007).

AAL and Talairach Daemon are limited in that they are based on a single subject's brain, and thus do not deal with anatomical variability across individuals, making them, in a sense, too deterministic. Anatomy is a variable that can be probabilistically presented on the common stereotactic platform. An alternative probabilistic macro-anatomical template, LPBA40, which was created based on 40 subjects with macro-anatomical segmentation at the gyrus level, is available (Shattuck et al., 2008) (Figs. 2B, E). It provides more probabilistic macro-anatomical information in MNI space. Meanwhile MNI152 has undergone an interesting innovation where the original 152 entries have been nonlinearly and iteratively transformed to form an integrated canonical brain with major sulci being preserved (ICBM152NLin; Fonov et al., 2011). While it provides a macroanatomical structure representing the general population, ready for visual inspection, it still lacks resources for macroanatomical labels. If the nonlinear version of MNI152 were equipped with AAL as is Colin27, it could develop into an unbiased canonical brain.

Additionally, a project lead by Zilles, which aims to probabilistically describe cortical anatomy, including histochemical structures, based on multiple postmortem brains in MNI space is underway (Amunts et al., 2007; Zilles and Amunts, 2010). This can be regarded as a probabilistic renewal of Brodmann's atlas in three-dimensional space. Now that the Matlab toolbox enabling probabilistic cytoarchitectonic mapping (Anatomy toolbox) is available for SPM, the fNIRS community can soon benefit from their achievement.

There is another approach to data standardization, called Freesurfer that is currently gaining popularity (Fischl, 2012). This freeware program segments the brain into white and gray matter, unfolds it onto the surface of a sphere, and deforms it to the standard brain-like shape with visible white- and gray-matter patterns. Freesurfer enables an intuitive grasp of the macroanatomical information, at least for an experienced researcher. Since Freesurfer is best appreciated with three-dimensional structural information, it has a high affinity to the DOT technique. Indeed, some pioneering fNIRS studies have adopted Freesurfer-based data presentation (Abdelnour and Huppert, 2010; Cooper et al., 2012), making it another option for standardizing spatial data for fNIRS.

Since most fMRI and PET data are presented in either MNI or Talairach space, fNIRS data are best appreciated when they are presented in these coordinate systems (and possibly in Freesurfer space in the near future).

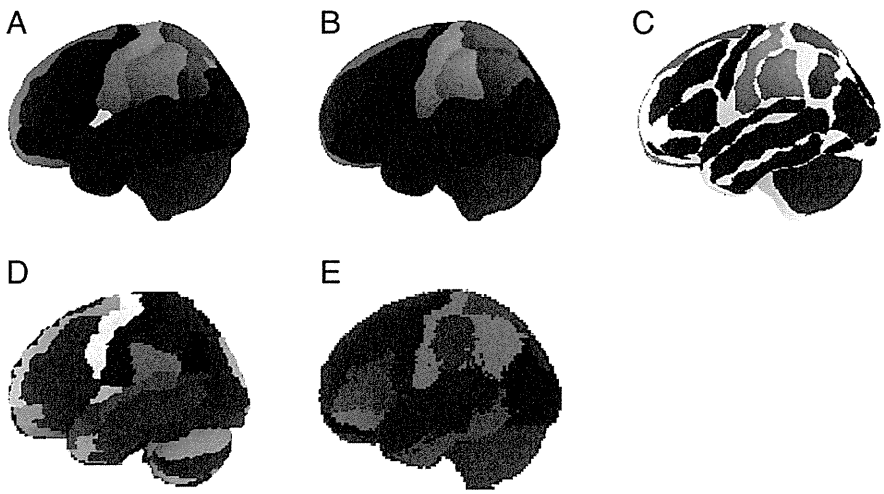

Fig. 2. Comparison between macro-anatomical atlases in MNI space. (A) AAL atlas based on the macro-anatomical segmentation of Colin27 is mode-filtered and projected onto NFRI_CB17 for use of fNIRS spatial registration. Some regions are integrated to maintain compatibility with the macro-anatomical segmentation in LPBA40. (B) LPBA40 atlas based on probabilistic macro-anatomical segmentation of 40 subjects is mode-filtered and projected onto NFRI_CB17 for use of fNIRS spatial registration. (C) AAL and LPBA40 atlases overlapping one another. The commonly labeled regions are depicted in different colors. 64.6% of macro-anatomically labeled voxels (42452/65745) of LPBA40 overlapped with those of AAL, while 69.2% of macro-anatomically labeled voxels (42452/61349) of AAL overlapped with those of LPBA40. (D) Unsmoothed original AAL. (E) Unsmoothed original LPBA40.

Such representation of fNIRS data enables inter-subject, inter-study, and cross-modal comparisons of neuroimaging data. However, it is not yet a common practice to present fNIRS data in these common stereotactic spaces due to the aforementioned technical shortcomings. Therefore, we will describe feasible strategies to address this.

Methods for describing scalp positions

The methods described above require acquisition of a structural image with MRI. However, this is not always guaranteed in typical fNIRS experiments. Even when an MRI is available, its use requires additional cost and effort, reducing the economical merits and convenience of fNIRS. In addition, spatial inference of group fMRI studies is based on a macro-anatomical atlas, and individual MRI scans are mainly used for transformation, not for anatomical inference based on individual cortical structures. Thus, the acquisition of an MRI may not be required for fNIRS group studies since here again MRI is used as a mediator for transformation to the standard brain space.

The fundamental problem of fNIRS in a standalone setting is that fNIRS data is primarily obtained from the head surface without structural information of the underlying brain. Thus, in order to spatially assess standalone fNIRS data, we must find the correspondence between the scalp location where an fNIRS measurement is performed and its underlying cortical surface where the source signal is located: fNIRS data obtained on the scalp should be registered to its underlying cortical surface. The lack of structural information in fNIRS essentially comes down to the issue of cranio-cerebral structural correspondence. Therefore, in a series of studies, we have aimed to solve the fNIRS spatial registration issue by establishing cranio-cerebral correspondence in the modern context of neuroimaging research. Before describing these methods, we will introduce the methods for describing scalp positions.

Currently, the international 10–20 system of electrode placement, which is the recognized standard for scalp electrode positioning for electroencephalography (EEG), is the most prevalent system for positioning electrodes (Jasper, 1958). This system describes scalp locations using relative distances between cranial landmarks with primary landmarks being the nasion (Nz), inion (Iz), and right and left preauricular points (RA, LA) (Supplementary Fig. 1). The 10–20 system then sets landmarks along the scalp systematically at 10% or 20% pitches (Supplementary Fig. 1). The 10–20 system assumes that there is a consistent correspondence between scalp locations and their underlying cerebral structures. Several studies have verified this structural correspondence using cadavers (Blume et al., 1974; Jasper, 1958), X-rays (Morris et al., 1986), CT-scans (Homan et al., 1987; Myslobodsky and Bar-Ziv, 1989; Myslobodsky et al., 1990) and MRIs (Gevins and Illes, 1991; Jack et al., 1990; Lagerlund et al., 1993; Okamoto et al., 2004a; Towle et al., 1993; Van den Elsen and Viergever, 1991).

With the advent of multi-channel EEG hardware systems, and the concurrent development of topographic data visualization methods and sophisticated tomographic signal source localization methods, there was an increased demand for extending the 10–20 system, which defines 21 electrode locations, to a system that allows for a higher-density of electrode settings. Thus, the 10–10 system, which defines 81 electrode locations, was proposed (Chatrian, 1985) (Supplementary Fig. 1). Its modified form has also been accepted as a standard of the American Clinical Neurophysiology Society (ACNS) (American Electroencephalographic Society, 1994; Klem et al., 1999) and the International Federation of Clinical Neurophysiology (IFCN) (Nuwer et al., 1998). Further, Oostenveld and Praamstra logically extended the 10–10 system to the 10–5 system, which has more than 300 electrode locations (Oostenveld and Praamstra, 2001) (Supplementary Fig. 1). For a detailed description of 10–20 and its derivatives, please refer to Jurcak et al. (2007).

Correspondence between 10–20 positions and the underlying macro-anatomical structure was established first by horizontally projecting 10–20 positions onto Brodmann's atlas (Homan et al., 1987). The two-dimensional projection has been extended to a three-dimensional method for 10–20 positions (Okamoto et al., 2004a) and 10–10 positions (Koessler et al., 2009). Meanwhile, correspondence to the MNI coordinate system has been made for 10–20 (Okamoto et al., 2004a) and 10–5 positions (Jurcak et al., 2007). It has been demonstrated that 10–10 positions are separated from one another across the scalp with standard deviations of a dozen mm, while 10–5 positions may be too dense to resolve scalp positions, especially in the occipital regions (Jurcak et al., 2007).

Although the link between scalp landmarks and MNI space are useful in computation, it is intuitively difficult to grasp the correspondence. Cutini et al. (2011) have made a unique contribution towards solving this problem by creating a real MNI152 brain and head model that can be used for fNIRS probe positioning and intuitive real-time mapping simulation by sliding an actual fNIRS probe holder over the physical head model. Although probe design and positioning can be simulated in a digital space, actual deformation of the probe holder and fine adjustments can be better realized on the real head model. This method has yet to be linked to many atlas resources in MNI, but such implementation is relatively easy, especially with the recent spread of 3D printers. Since structural data for standard brains are available on-line, they can be ready for 3D printing after some data conversion using computer-assisted design (CAD) software packages.

Registration of fNIRS data to a subject's own structural image

Regardless of the modality, spatial registration is a fundamental process in neuroimaging. Functional and structural images are obtained differently. For example, an fMRI image is obtained through a protocol called EPI, which takes advantage of the paramagnetic nature of deoxygenated hemoglobin (deoxy-Hb) to capture Blood-Oxygen-Level-Dependent (BOLD) signals (reviewed in Bandettini, 2012). A structural image is obtained as a T1-weighted image that depicts tissues with different fat contents to contrast the gray and white matter of the cortices. They usually have different resolutions, with functional images generally around 5-mm voxels, and structural images around 1 mm (Friston et al., 1996). Both are continuous images consisting of thousands of voxels. Both images are then merged through a process usually called "co-registration", referring to the merging of two or more images (Ashburner and Friston, 1999). This is relatively easy: since the two images are obtained in the same space using the same scanner, the head measurements at different times should match by rigid body transformation. Co-registration produces a functional image of a subject that is visualized over his/her brain.

If a researcher has access to an MRI scanner, a subject's fNIRS data can be co-registered to his/her own structural MRI. This can be executed in several ways, but the essential idea is the same: fNIRS data obtained in a real-world space is merged onto the structural MRI obtained in another real-world space. The most straightforward way to carry this out is to place markers (e.g., vitamin-E capsules or pine-nut beads) to indicate fNIRS probe or channel positions, and take the structural MRI together with these markers (Okamoto et al., 2004a). Then, fNIRS probe or channel positions can be expressed directly on the subject's MRI. Alternatively, fNIRS probe or channel positions are recorded by a three-dimensional (3D) digitizer (typically magnetic) together with the positions of at least three scalp landmarks. The scalp landmarks should be detectable both on the subject's head and on his/her MRI. Technically few points can fulfill this requirement. Therefore, the bilateral preauricular points and the nasion are most often used. Mediated by these landmarks, fNIRS probe or channel locations are transformed to MRI with a rigid body transformation consisting of rotation and translation (Fig. 3).

Once probe/channel locations are described on the real-world space that the subject's MRI belongs to, fNIRS data are either expressed as discrete channel-wise data where functional data (e.g., relative signal change of oxygenated hemoglobin) are bound to channels (Maki et al.,

1995) or a continuous topographic image where a two-dimensional continuous pixel image is created by interpolation (Watanabe et al., 1996). However, since these data are presented on the scalp, not on the cortex, fNIRS data registration goes beyond simple co-registration, and undergoes distinct procedures involving data projection onto the cortical surface (Fig. 3). Projection can be carried out either by searching for the nearest cortical point of a given scalp point, drawing a vertical line from a tangential plane of the scalp point, or drawing a line to a central location such as the centroid of the brain (Okamoto and Dan, 2005). Alternatively, a three-dimensional functional image is reconstructed based on the optical properties of head and brain tissues, and by adopting the photon-measurement density function to each channel consisting of a source–detector pair (Arridge, 1999; Boas and Dale, 2005). Accordingly, signal source distribution is estimated on the subject's MRI with or without depth information in DOT and DOI, respectively (Bluestone et al., 2001; Culver et al., 2003). This method is usually implemented using optional software packages offered by fNIRS constructors. Free software packages such as HomER2, NIRS-SPM and our in-house MATLAB tools are also available for this purpose (Huppert et al., 2009; Ye et al., 2009).

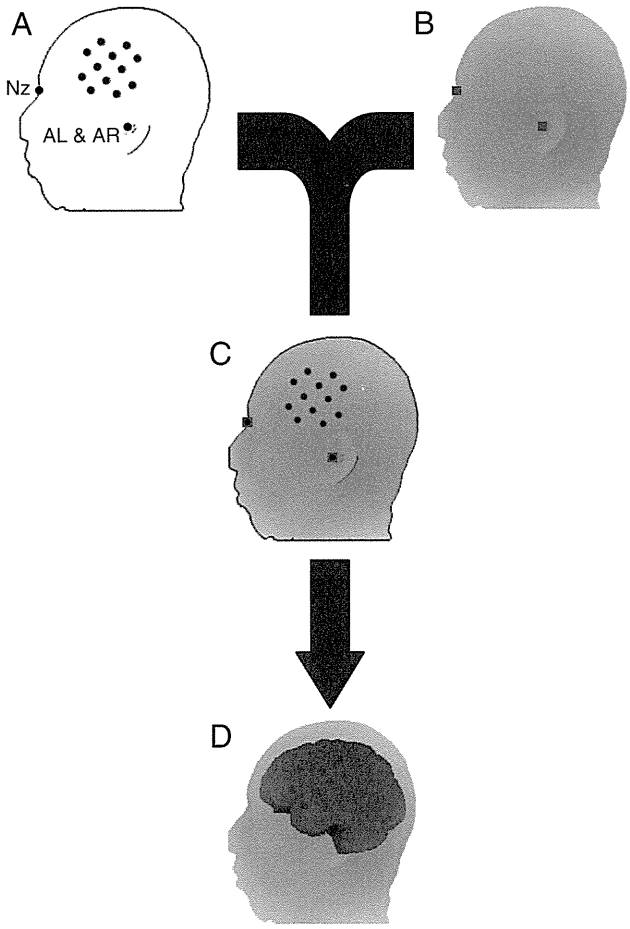

Fig. 3. Registration of channel-wise individual fNIRS data to a subject's own structural image. (A) Multichannel fNIRS channel (blue dots) and reference scalp landmark (black dots) positions on the scalp are measured in a real-world coordinate system using a 3D-digitizer. Nz stands for nasion; AL, left preauricular point; AR, right preauricular point, which is located on the other side of the head. (B) Structural image of the head and brain is obtained using MRI in another real-world coordinate system. The three scalp landmarks (red squares; one on the other side of the head) are also identified manually. (C) The 3D-digitized reference scalp landmarks (black dots) are merged onto the corresponding landmarks on the MRI using rigid-body transformation: thereby, fNIRS positions are also transformed and co-registered onto the subject's own MRI. (D) Finally, the fNIRS channels on the scalp are projected onto the cortical surface (smoothed for better visibility).

Group analyses with direct co-registration to MRI

While a researcher may have a subject's own structural MRI and fNIRS probes/channels co-registered for each subject and can normalize the MRIs to the MNI standard brain, expressing group fNIRS data in the standard brain is not straightforward. For channel-wise analyses, once real-world coordinates of the channels and probes compatible to the structural MRI are available, we would like to report them in the MNI coordinate system. Since normalization is optimized for fMRI, we must perform additional steps to do this (Fig. 4). First, we spatially normalize each subject's MRI head image to the MNI standard brain template using SPM and extract the inverse deformation field matrices. These matrices are used for normalizing the subject's head images from the pre-processing report produced by SPM (Singh et al., 2005). Next, we apply these inverse deformation field matrices to the fNIRS probe and channel positions, and their cortical projections, in order to obtain their coordinate values in MNI space (Tsuzuki et al., 2012). The toolboxes for these procedures are available on our website (http://www.jichi.ac.jp/brainlab/tools.html).

Subsequently, each channel position across subjects in MNI space is averaged to yield the most likely MNI coordinate values (Fig. 5). However, we must be mindful that transformation of a specific scalp/cortical point to the standard brain space entails an error factor intrinsic to transformation. For example, F3 is regarded as the same scalp position across subjects while the cortical projection point for F3 may be transferred to a point with MNI coordinate values of [−35, 49, 32] in one subject but to a nearby point with different coordinate values in another subject. Thus, variability intrinsically associated with spatial transformation should be addressed. Specifically, variability statistics such as standard deviation (SD) along the x, y, and z axes or composite SD (cSD) in terms of radius describes how stable the estimation is (Okamoto et al., 2004a; Singh et al., 2005). In typical multi-channel measurements in adults, cSD is several to a dozen or so mm. Therefore, for a typical fNIRS channel density that does not provide overlapping measurements, distinct channels can be associated fairly well with, for example, a single cortical gyrus or with the Brodmann area.

Here we must reconsider the prerequisite of channel-wise analyses in group studies: channel locations can be considered similar across subjects. As long as the set of probes is small enough and reproducibly placed across subjects, each channel should represent a distinct location on the brain, and thus the spatial identity of a channel is preserved.

However, the independence of a channel is not always guaranteed. With more channels, placement is less reproducible because of variability in head shape and size. An extreme case can be found in whole-head measurement (Koizumi et al., 2003), where the spatial identity of a channel is no longer maintained. In such cases, multi-channel data may be integrated into a region of interest (ROI) (Yanagisawa et al., 2010). For example, if three channels are expected to be located over the left angular gyrus in subject 1, four in subject 2, and two in subject 3, they are respectively grouped to represent the left angular region of each subject (Okamoto et al., 2009). This is also realistic for reproducible channel-wise data because we are not necessarily interested in the functions of channels that are arbitrarily set, but rather in those of macro-anatomical regions.

However, we may have to consider how valid macro-anatomy in a group study is. Even with fMRI, where the macro-anatomical features of each subject are obtained and preserved in MNI space, macro-anatomical information is lost during averaging among subjects. In general, once functional data is expressed in MNI space, macro-anatomical information is regained in reference to anatomical atlases, such as AAL, compatible with MNI space. However, we must remember that AAL is based on the macro-anatomy of a single subject, meaning that functional inferences bound to macro-anatomy in most fMRI studies are based on the particular macro-anatomical structure of that subject. This is an often-neglected reality of fMRI analyses. Nevertheless, here again we are usually interested in functional characteristics of a certain macro-

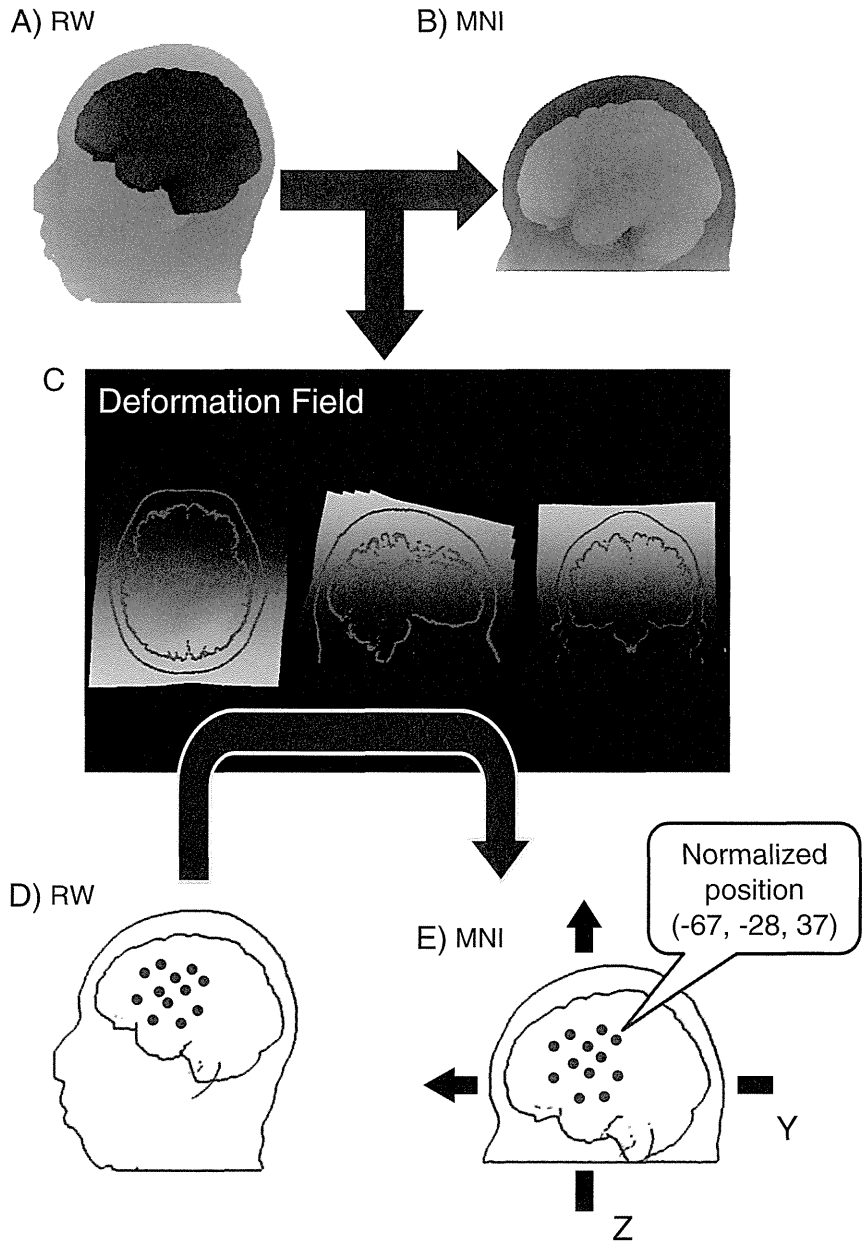

Fig. 4. Normalization of channel-wise individual fNIRS data to the standard brain space. A subject's own MRI in a real-world (RW) coordinate system (A) is normalized to the MNI 152 template to be expressed in MNI space (B) using the SPM program. The deformation field that reflects warping transformation matrix from RW to MNI spaces is extracted (C). Discrete fNIRS channel position data in RW space (D) are transformed to MNI space (E) using the deformation field. Eventually, coordinate values of each fNIRS channel are available in MNI space (Matlab toolbox is available at http://www.jichi.ac.jp/brainlab/tools.html).

anatomical structure, and actually, the macro-anatomical structural differences between individually based AAL and multi-subject-based probabilistic LPBA40 are not substantially different (Fig. 2C). In Fig. 2C, the colored island-like patches represent commonly labeled regions and denote core parts of gyri, consisting of two thirds of the lateral cortical surface. The area that appears as the background in this image corresponds to border regions between gyri. Thus, while group analyses of fMRI data for macro-anatomical functional inference seems reasonable, at least at the gyrus level, inference for the sub-gyrus level may be in question.

Returning to fNIRS, we next consider group analyses of continuous image data, which are either obtained though interpolation or image reconstruction (Fig. 6). In fMRI data, since whole-to-whole transformation is carried out from an individual to the standard brain, the size and orientation of the functional data are intrinsically defined by those of the standard template. In continuous fNIRS image data, individual differences in the scalp shape and size lead to different shapes, sizes and orientations of the continuous image data. While center regions of the continuous image are common across subjects, peripheral regions may not overlap among subjects. This is partially resolved in the NIRS-SPM software package (Ye et al., 2009), which can adjust the degree of overlap (e.g., allowing a region where 60% of data overlap). How to handle the overlap requires more study. For now, center regions that are common among all subjects can be conservatively selected.

Another problem involved in continuous image integration in the standard space is effective spatial resolution, which is often referred to as resolution elements (resels) (Nichols, 2012). Typically, a continuous image with a voxel size of 1 mm is created from more sparsely arranged probes at either a fixed distance of typically 3 cm or differential distances of a few to several cm for image reconstruction in DOT/DOI. Currently,

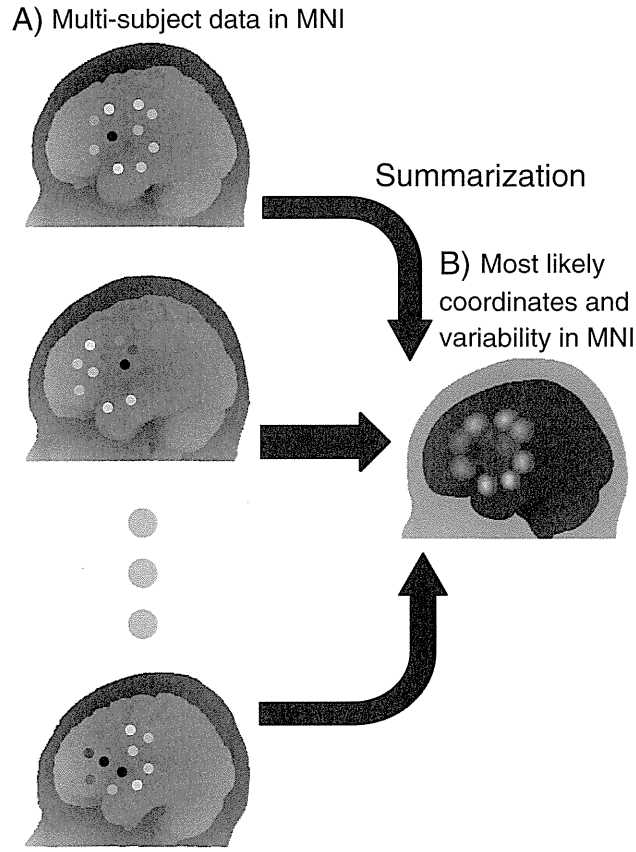

Fig. 5. Integration of channel-wise multi-subject fNIRS data in MNI space. After the process described in Fig. 1, channel-wise fNIRS data for each subject are expressed in MNI space. By repeating this procedure, multi-subject data are available in MNI space (A). They are summarized in MNI space (B), where the coordinates for channel positions are averaged to yield the most likely channel positions (centers of the circles), and variability as expressed in composite standard deviation (radii of the circles). Colors represent activation in a jet scale (red is more activated and green is less activated). Activation patterns are correspondent to those in Fig. 6. Note: this procedure is also applicable for multi-subject data obtained by the probabilistic registration method as described in Fig. 7.

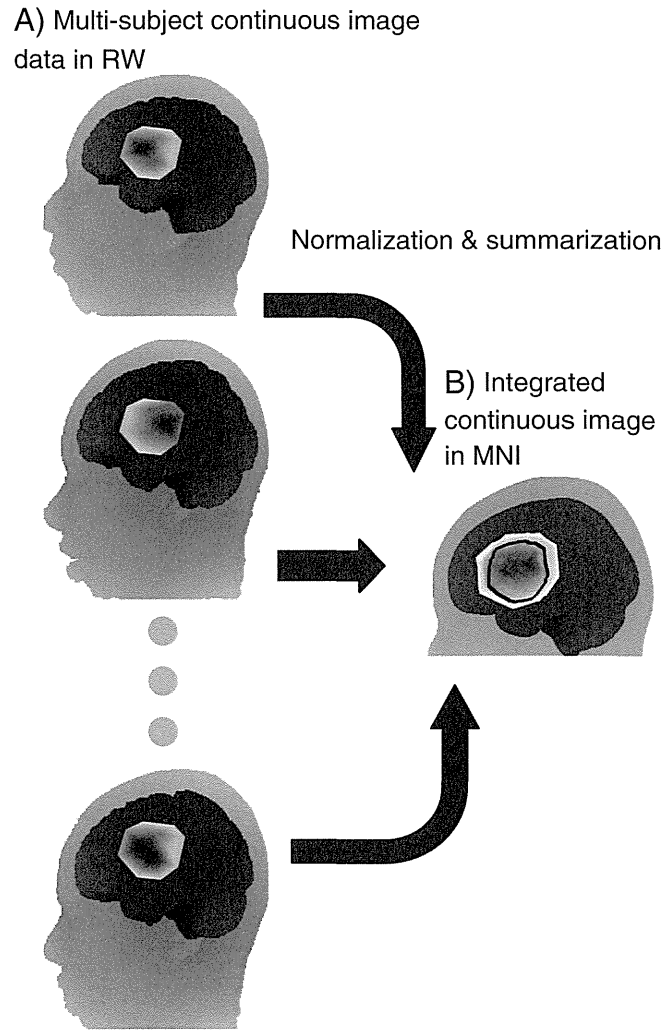

Fig. 6. Integration of continuous image fNIRS data in MNI space. A continuous image is created in a real-world (RW) space for each subject using either interpolation or image reconstruction methods (A). Each image is normalized to MNI space and averaged to one another to yield an integrated continuous image in MNI space (B). The outer edge represents a region that is covered by at least one subject, the inner black boundary represent the region that is covered by all subjects (15 in this simulated data). Colors represent activation in a jet scale (red is more activated and green is less activated). Activation patterns are correspondent to those in Fig. 5.

the finest experimentally resolved resolution of fNIRS data reconstructed in high-density DOT has reached several mm, which is comparable to fMRI resolution (Eggebrecht et al., 2012). However, the effective resolution of typical fNIRS should be greater than that, and, obviously, functional inference at a 1 mm voxel would involve over estimation. Given the currently prevailing convention that functional inference of fMRI group studies is dependent on the resolution of the anatomical labeling tool, functional inference of continuous fNIRS images would also be limited by the same factor.

Robust functional inference for continuous fNIRS image data can be achieved with ROI analyses. One method is to set center coordinate values (e.g., [−67, −26, 30] for the left supra-marginal gyrus), and extract neighboring voxels (e.g., those within 2 cm of the center) to represent a functional status in the ROI. The advantage of this approach is that multiple ROIs of the same size can be set across cortical regions. Note that setting a ROI by integrating channels or voxels is equivalent to applying a spatial filter for smoothing, and thus different ROI sizes result in different degrees of spatial filtering (e.g., the signal to noise ratio of a ROI twice as large as another, can be improved by $\sqrt{2} = 1.4$). Another method is to refer to a macro-anatomical atlas to extract voxels belonging to a given macro-anatomy (e.g., selecting all voxels with the label of right SMG in AAL). This seems a straightforward method, but we should be aware that extreme differences in ROI sizes entail different degrees of spatial smoothing.

Probabilistic registration for standalone fNIRS data

Often the availability of an MR scanner is limited, and even when one is available, mandatory co-use of fNIRS and MRI would reduce the convenience of fNIRS measurements, and impose extra burdens on the subjects. Thus, as a practical alternative, we developed a probabilistic registration method that utilizes MRIs stored in a reference database rather than the subjects' own MRIs, and probabilistically registers fNIRS probe or channel positions onto a standard brain template (Singh et al., 2005) (Fig. 7). We first constructed a reference database containing the head and brain MRIs as well as the 10–20 standard positions of 17 individuals registered to MNI space. This database serves as an anatomical reference in place of a subject's own MRI. We applied an affine transformation of the fNIRS channel coordinates on the subject's head (real-world space), which were obtained with a 3D magnetic digitizer, to the reference heads in the database (MNI space), using 10–20 standard positions as landmarks. Then, we registered head surface points to their corresponding cortical surfaces in MNI space. For group analysis, we obtained a multi-subject distribution of cortical points corresponding to a given fNIRS channel on the head surface. In addition, we obtain the most

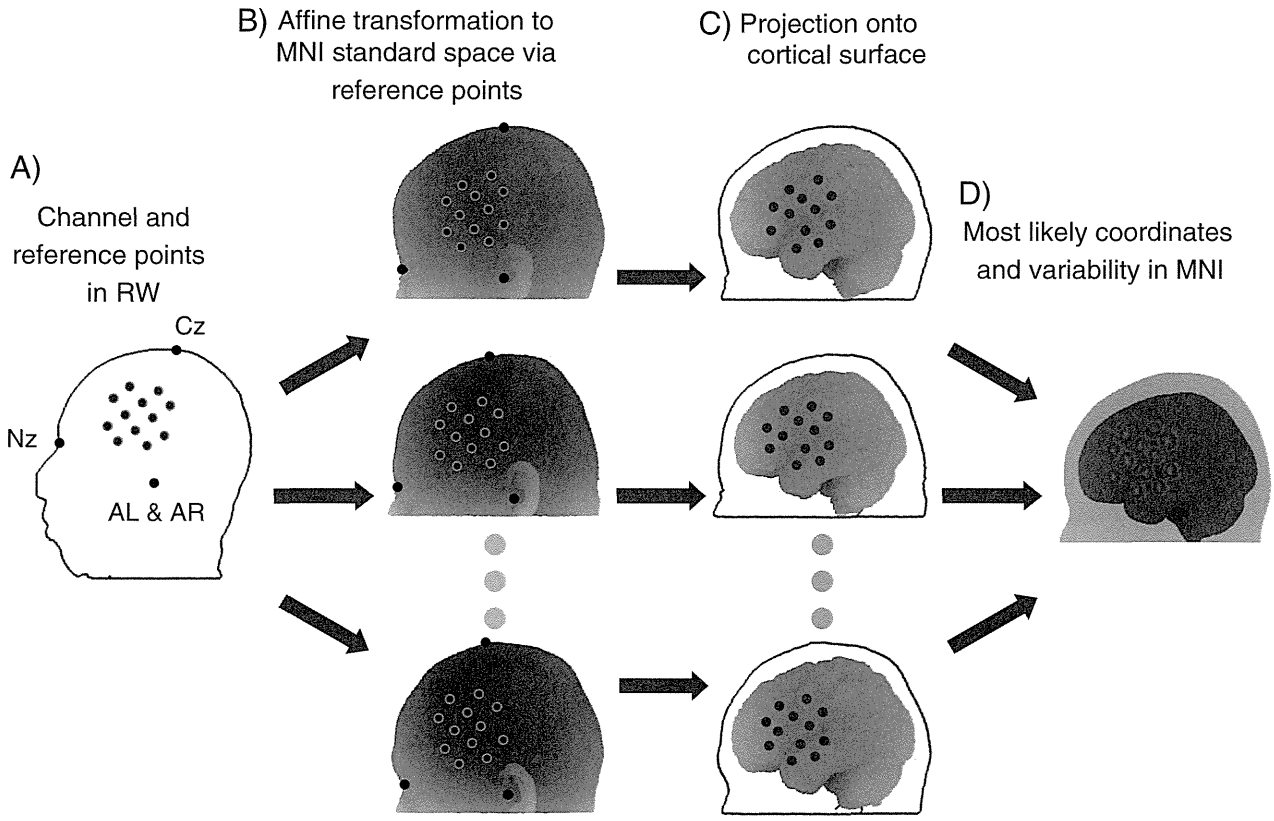

Fig. 7. Probabilistic registration of single-subject data without MRI. (A) Positions for channels and reference points in real-world (RW) space are measured using a 3D-digitizer. The minimum number of reference points is four, as in this case, where Nz (nasion), Cz, and left and right preauricular points (AL and AR) are used. Alternatively, whole or selected 10/20 positions may be used. (B) The reference points in RW are affine-transformed to the corresponding reference points in each entry in reference to the MRI database in MNI space. (C) Channels of the scalp are projected onto the cortical surface of the reference brains. (D) The cortically projected channel positions are integrated to yield the most likely coordinates (average: centers of spheres) and variability (composite standard deviation: radii of spheres) in MNI space. Single-subject data may be subsequently subjected to group analyses as described in Fig. 5.

likely estimate of the cortical point in a group of subjects, as well as cSD representing error effects due to variability across subjects and across reference brains. The cSD of the projected cortical point obtained from the proposed registration process is on the order of millimeters when fNIRS probes are reproducibly set on the scalp (Tsuzuki et al., 2012). This is sufficiently accurate for most functional mapping performed at the gyrus level.

In order to perform probabilistic registration based on affine transformation on three-dimensional space, we need at least four distinct reference landmarks on the scalp. However, a human scalp is not optimized for probabilistic registration. Although three landmarks, most often the Nz and preauricular points, are relatively easy to determine accurately (Jurcak et al., 2007), the fourth position is hard to find and entails considerable variability. The most feasible scalp landmark for realizing a balanced arrangement of the landmarks with sufficient vertical height is Cz of the international 10–20 system. However, determination of Cz is dependent on Iz, leading to ambiguity due to Iz's variability.

Thus, a registration method that avoids Iz and Cz is greatly desirable. To meet this demand, we have introduced an anchor-based probabilistic registration method: a novel method utilizing affine transformation via three distinct cranial landmarks (i.e., Nz and the left and right preauricular points) and an additional anchor point, which can be obtained from anywhere on the scalp (Tsuzuki et al., 2012). The essence of the anchor-based probabilistic registration method lies in its partial use of a spherical coordinate system. Using the three cranial landmarks, we can define a distinct plane from which we can further define a spherical coordinate system. Specifically, we set the midpoint between two preauricular points (AR and AL) as the origin of the spherical coordinate system, and so define the reference plane that passes through this origin toward Nz. Accordingly, transformation from a subject's scalp to a reference head's scalp can be executed in reference to the azimuth and elevation angles. However, the anchor point, transferred to a reference head does not have any link to MNI space. This is solved by extracting the deformation field used for transforming the reference head to MNI space (Ashburner and Friston, 1999; Ashburner et al., 2000;) and using it to transform the anchor point.

Anchor-based probabilistic registration is as stable as conventional probabilistic registration. Comparisons among anchor-based probabilistic registration, conventional probabilistic registration, and SPM-based registration via co-registration to a subject's own MRI revealed that intra- and inter-method variabilities were comparable, with both on the order of millimeters (Tsuzuki et al., 2012). Thus, it is suggested that the absence of a subject's own MRI does not necessarily decrease the accuracy of the spatial registration of fNIRS probes or channels to MNI space in group analyses. In an actual experimental situation, all an experimenter needs to do is to click a 3D-digitizer somewhere on the top of the scalp. This substantially reduces the experimental burden by omitting tedious measurements of Iz and, subsequently, Cz. This method is especially useful in clinical studies where experiment time is often limited.

Application of probabilistic registration to DOT

One promising application of probabilistic registration and its derivatives is the transference of data to DOT, the tomographic variant of fNIRS, which utilizes a relatively large number of sources and detectors to reconstruct 3D images of brain activation (Bluestone et al., 2001; Boas et al., 2003; Culver et al., 2003). DOT uses short and long distance measurements to provide depth resolution and enables separation of superficial scalp signals from deeper brain signals. The spatial resolution

of DOT has been improved to the point where it can construct a detailed retinotopic map in the visual field (Zeff et al., 2007).

However, in order to create a 3D image, DOT generally requires subject-specific spatial priors of the head anatomy that have been segmented into several layers of tissue typically including skin, skull, cerebrospinal fluid, gray matter and white matter (Barnett et al., 2003). This requires a structural MRI of the subject, and the additional segmentation, registration and image reconstruction processes are computationally demanding. This obviously conflicts with the economical merits and convenience of fNIRS. However, this can be solved by applying probabilistic registration methods. Thus, rather than using a subject's own MRI, use of the standard atlas was explored (Custo et al., 2010). Colin27 was selected as the atlas as it is normalized to MNI space and has stable anatomical features so that it can be stably segmented into tissues (Collins et al., 1994). Also, Colin27 is the source of AAL, and thus is optimized for automatic anatomical labeling (Tzourio-Mazoyer et al., 2002). This MRI-free approach to obtaining optical images is based on registering a selected atlas to the subject head surface using probabilistic registration via 10–20 positions and solving the photon migration forward problem on the registered atlas. For the hemodynamic response to median-nerve stimulation, both reconstructed DOT images using the subject-specific brain anatomy and those using the atlas were able to locate the activation focus within the post-central gyrus correctly.

In a subsequent validation study, the diffuse optical images of simulated cortical activation in 4000 distinct regions for 32 subjects were reconstructed using a registered atlas and compared with those obtained using a subject's true anatomy (Cooper et al., 2012). When using a subject-specific MRI, localization error, which is due to diffuse optical image reconstruction, was 9 mm. However, when using a registered atlas, localization error was 18 mm. This error is due to a combination of imperfect registration, anatomical differences between atlas and subject anatomies and the localization error associated with diffuse optical image reconstruction, and thus the cost of using the atlas is 9 mm. The simulated activation had a radius of 10 mm. Since this may be more confined than general activation enrolled in typical cognitive and physical tasks, the localization error may be buried in relatively wide activations. Although a more detailed examination is necessary, it is predicted that atlas-guided DOT would be useful for gyrus-level inference. Given that photon migration simulations in DOT have been accelerated using a GPU-based Monte Carlo algorithm (Fang, 2010), the computational cost of DOT will be less of a problem when the atlas-based technique is used. Thus, we expect that DOT, as well as conventional fNIRS, will benefit from their convenience and economical merits, and acquire a wider range of applications.

Virtual registration

The 3D-digitizer registration methods described above allow the registration of fNIRS channel data onto MNI coordinate space even when a subject's own MRI is not available. However, this system still requires 10–20 landmarks and that the probe positions on a subject's head be carefully measured with a 3D-digitizer in order to reproduce their placement on the MR images of the reference head/brain database. This imposes a certain burden on subjects, and thus limits the application of the probabilistic registration method in some clinical situations. To circumvent this, we have devised a 3D-digitizer-free method for the virtual registration of fNIRS channels onto the stereotactic brain coordinate system (Tsuzuki et al., 2007) (Fig. 8). However, note that this method works only when probe holder positioning and deformation are reproducible across subjects. Essentially, this method allows us to place a virtual probe holder on the scalp by simulating the holder's deformation and by registering probes and channels onto reference brains in place of a subject's brain. First, we constructed a holder deformation algorithm for commercially available probe holders. Next, we simulated the registration of virtual holders on synthetic heads and brains that represent size and shape variations among normal adults. We normalized the registered positions to MNI space. With one thousand repetitions, we statistically estimated the most probable MNI coordinate values together with the errors associated with their estimation. As in the case of the 3D-digitizer method, the standard deviation was on the order of millimeters across the scalp. Thus, the virtual registration method realized the spatial registration of completely stand-alone fNIRS data onto MNI space without using supplementary measures. This method is also applicable for individual data, but the lack of size information can lead to large variability. Thus, for better individual estimation, head size information, such as circumference, would preferably be implemented in simulation (manuscript in preparation).

However, this is based on the careful placement of the probe holder and a detailed examination of the holder shape and deformation. Even a slight deviation in holder shape, such as an insertion of a spacer with a thickness of several millimeters between the holder and the head, may alter the results. Thus, the description of probe settings should be as exact as possible. Although it is automated, the current procedure requires rather complicated parameter settings depending on the types of holders actually used. Thus, we created a virtual registration library for common probe placements in adult subjects, where MNI coordinates and macro-anatomical estimation for fNIRS channels are available.

Implementation of probabilistic registration in software packages

As fNIRS use expands, there is an increasing need for software packages to process the data. Currently there are three major freeware packages that work on Matlab. These packages have adopted probabilistic registration tools and thus can perform spatial registration to MNI space for standalone fNIRS data. We will briefly introduce how these packages utilize probabilistic registration.

First, HomER2 is an integrative fNIRS data processing tool with a user-friendly graphical user interface (GUI). The first version was developed by Huppert et al. (2009), and the most recent version is maintained by Dr. Boas's lab at Massachusetts General Hospital. HomER2 offers an interactive spatial registration interface with 10–20 landmarks preset in a GUI. Users can design probe arrangements virtually with the GUI. HomER2 is compatible with 3D digitizers and thus can perform probabilistic registration for channel-wise analyses and reconstructed continuous images. HomER2 also provides users with "recipes" with which they can define sequences of toolboxes for data processing such as temporal filters, generation of experimental blocks, independent component analyses, GLM, and so on. This allows flexible spatiotemporal data analyses for fNIRS.

Second, NIRS-SPM offers statistical parametric mapping tools for fNIRS (Ye et al., 2009). It generates continuous image data from discrete channel data using inhomogeneous spline interpolation kernels either from individual or group data. When used for standalone fNIRS data, NIRS-SPM transforms the functional image to MNI space using probabilistic registration in reference to 3D digitized data of probe and 10–20 landmark positions. For individual data, it statistically processes time-line data using a regression to basis function with a general liner model (GLM) and adopts Sun's tube formula for adjusting multiple voxel comparison (Sun, 1993; Sun and Loader, 1994). For group analyses, continuous functional images created for each individual are merged together in MNI space and are subjected to second level analyses using a GLM with correction for multiple voxel comparison using the random field theory.

While these two packages offer relatively standardized analytical flow, the final package, Platform for Optical Topography Analysis Tools (POTATo), offers flexible modulation capability upon user demand (Katura et al., 2008). POTATo itself offers no standardized procedures, but provides users with recipes, as does HomER2. The main difference seems to be that POTATo put emphasis on the flexibility of recipes so that new, custom-made functions can be incorporated relatively easily.

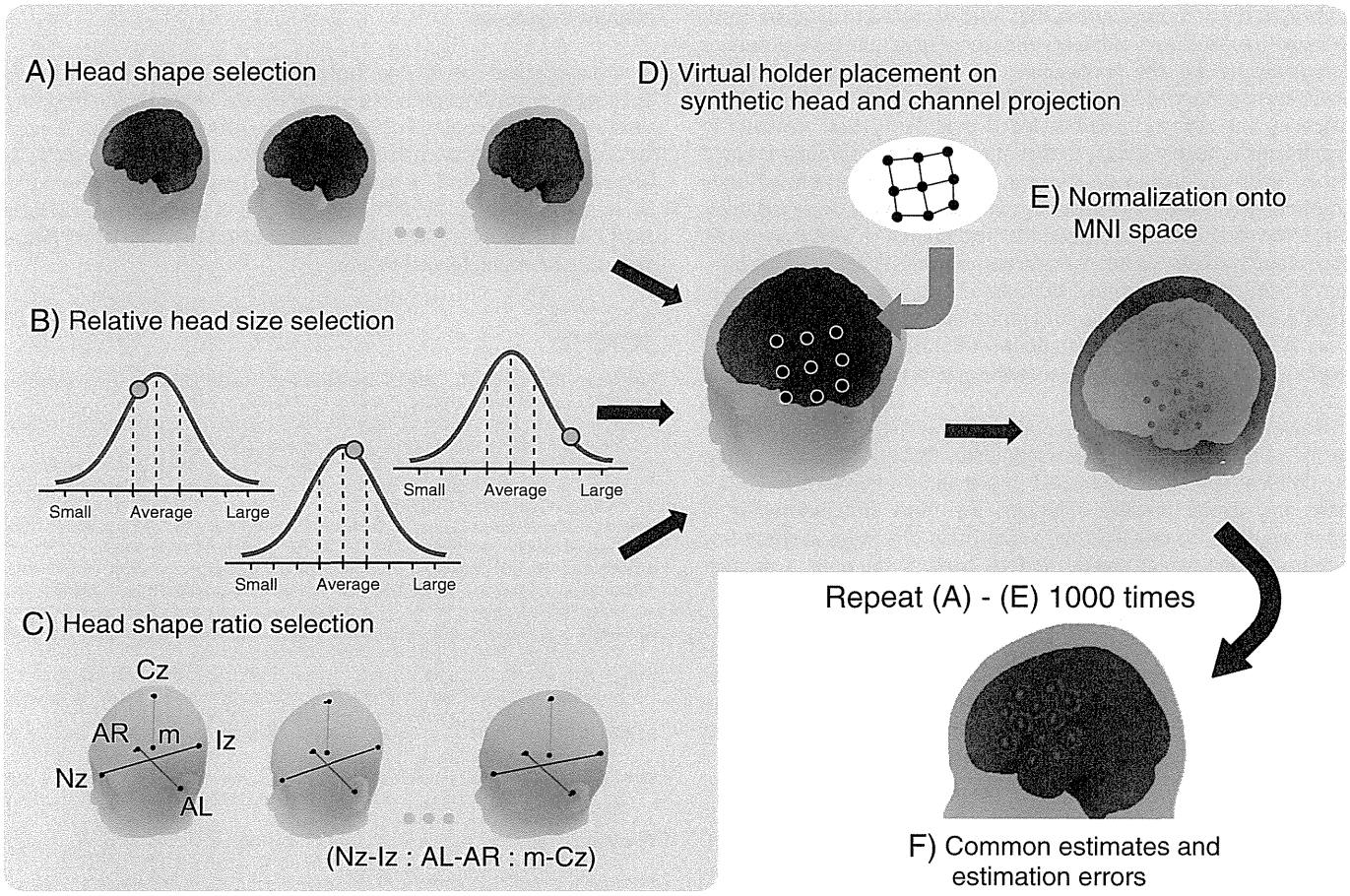

Fig. 8. Virtual registration of multiple-subject data without MRI or a 3D-digitizer. A synthetic head and brain is created from resampling a reference MRI to provide a global head and brain shape (A), relative head size (B), and head shape ratio (C). In (C), m represents the gravity center of AR, AL, Nz and Iz. On the synthetic head, a virtual fNIRS probe holder is placed based on the assumption that probe holder deformation and placement is reproducible (D). From the fNIRS probes (black dots in D), channels are defined as their inter-probe mid points (process not shown). The channels are projected on the synthetic brain and normalized onto MNI space (E). This process is repeated one thousand times to yield the most likely estimates (average: the centers of red circles) and estimation errors (composite standard deviation: the radii of the circles). For a single-subject estimation, the head size in (B) may be fixed to the subject's head size.

Probabilistic registration and virtual registration toolboxes can be incorporated into POTATo in a stable manner (available at http://www.jichi.ac.jp/brainlab/tools.html). Depending on the user's needs, POTATo can process channel-wise data or continuous image data for both individual and group analyses.

Although our toolboxes for probabilistic registrations are available on our website, they are offered as basic Matlab functions with a minimum GUI so that developers can easily integrate them into their own software packages. Relatively experienced users with Matlab literacy may use our native toolboxes, but others may prefer to use them through the software packages introduced above.

Registration of infant and child data

One challenge to be tackled in the near future is the development of registration methods for infant and child fNIRS data. There is no established standard stereotactic system for processing infant brains, but many important initial advances have been made in recent years. The prerequisite for the standard stereotactic system is a probabilistic brain template that can be used for segmentation and normalization, and this was first presented by (Altaye et al., 2008) based on the MRIs of 76 infants at 9 to 15 months old, yielding segmentation of gray matter, white matter and CSF. In addition, the development of age-specific templates has been made for neonates to 4-year-old children (Sanchez et al., 2012), infant brains at any given stage between 29 and 44 gestational weeks (Kuklisova-Murgasova et al., 2011), and 4.5- to 18.5-year-old children (Fonov et al., 2011), allowing segmentation of gray matter, white matter and CSF. Another group has created an average-shape atlas made by aligning 68 neonatal brains to MNI space and averaging them after iterative affine and nonlinear transformation (Shi et al., 2010). Although this atlas included 76 parcellated brain regions, their correspondence to macro-anatomy remains unclear. Macro-anatomical segmentation of neonatal and early infant brains is extremely difficult because only lower contrast images can be obtained compared to adult head scans. Stable macro-anatomical segmentation is only possible from the age of 2: Gousias et al. (2008) succeeded in segmenting 2-year-old brains into 83 regions. While lobe-level macro-anatomical segmentation seems fairly successful, more elaboration is necessary for gyrus-level segmentation.

Reflecting the difficulty of making anatomical atlases specific to infants and young children, extrapolation of an adult atlas to young brains has been implemented as a practical compromise. Shi et al. (2011) created a longitudinal deformation field to transform adult brains to infant brains, through which they projected AAL to neonate, 1-year-old and 2-year-old brains.

We also took a similar approach in our collaboration studies to apply probabilistic or virtual registration procedures to the transformation of scalp fNIRS channels to the cortical template in MNI space based on the assumption that the relative macro-anatomical structural patterns of young infant and child cortices are similar to those of adults. This assumption is based on the study by Hill et al. (2010), which showed that the surface-based atlas of the cerebral cortex in term infants is similar to that of an adult in the pattern of individual variability. Specifically, they have established a population average surface-based atlas of the human

cerebral cortex at term gestation. This atlas was used to compare cortical shape characteristics of infants with those of adults. Cortical surface reconstructions for the hemispheres of 12 healthy term gestation infants were generated from structural MRI data. Based on these reconstructions, the authors have concluded that the cortical structure in term infants is largely similar to that in adults. This assumption should also be valid in children (7–8 years), whose atlas-transformed brain morphology is relatively consistent with that of adults (Burgund et al., 2002). To validate the assumption that registration to MNI stereotactic space is applicable to the infant brain, we performed the virtual registration of fNIRS probe and channel locations of 3- to 6-month-old infants to a neonate AAL atlas (Shi et al., 2011) transformed to MNI space (Altaye et al., 2008). The virtual registrations with adult and neonate brains showed that they are macro-anatomically comparable (Watanabe et al., 2013).

However, this approach is not optimum. Since fNIRS has good potential for cultivating pediatric developmental functional neuroimaging, this problem should be addressed in a manner optimized for fNIRS. There are several possible solutions, the most straightforward of which would be to establish and verify brain templates representing various developmental stages, and to express them in a manner compatible with the MNI coordinate system. As described above, many templates have been produced, but they have different degrees of compatibility with MNI space without satisfactory access to macro-anatomical atlases. Integration of or an inter-link between different systems should be established in the near future. Alternatively, spatial data could be standardized in relative scalp–coordinate systems with direct macro-anatomical links. One plausible solution may be to utilize a spherical coordinate system that was once introduced for standardizing electroencephalography data in the early 90s (Lagerlund et al., 1993; Towle et al., 1993). Also, it would be possible to express scalp and cortical positions via the international 10–20 system or its derivatives. These processes necessarily require manual tracing of macro-anatomical structures at the gyrus level rather than automatic macro-anatomical segmentation. Since macro-anatomical manual tracing for longitudinal volumetry of developmental brains has been implemented in recent years (Tanaka et al., 2012; Uematsu et al., 2012), we can expect substantial progress in the near future.

Concluding remarks

Having undergone two decades of development, fNIRS now seems to be acknowledged among researchers as a feasible neuroimaging modality.This imposes that fNIRS can no longer exist in a vacuum, but should be linked with other imaging modalities to promote brain science. The advent of functional neuroimaging techniques most exemplified by fMRI has revolutionized brain science. Essentially, we can now visualize how the brain regions are activated or connected to each other. However, fMRI measurement constrains subjects in a scanner. Conversely, fNIRS, being compact and allowing more freedom of motion, has the potential to liberate functional neuroimaging from the laboratory into the real world. However, this does not mean the liberation of fNIRS in a methodological context, and isolated development of fNIRS may result in a great loss to the neuroimaging community. Therefore, to facilitate data sharing and cross-referencing among the neuroimaging community, we have devised methods to register spatial fNIRS data onto the common stereotactic brain coordinate systems. By describing fNIRS data on the common stereotactic coordinate systems, we can compare fNIRS data to functional and structural data obtained by other neuroimaging modalities. In turn, fNIRS data can also be referred to by other modalities. We believe such cross-modal interaction of fNIRS is a key factor for promoting the development of fNIRS research, and for furthering neuroimaging research as a whole in the decades to come.

Supplementary data to this article can be found online at http://dx.doi.org/10.1016/j.neuroimage.2013.07.025.

Acknowledgments

We appreciate Haruka Dan, Toshifumi Sano, and Yukie Hirokawa for assisting in manuscript preparation, and Hiroko Ishida for administrative assistance. We appreciate ELCS—English Language Consultation Services for proofreading the manuscript. This work was supported in part by the Grant-in-Aid for Scientific Research from the Japan Society for Promotion of Science (22242012, 23390354, 2370885, and 23650217), and Health and Labor Sciences Research Grants, Research on Psychiatric and Neurological Diseases and Mental Health.

References

Abdelnour, F., Huppert, T., 2010. A random-effects model for group-level analysis of diffuse optical brain imaging. Biomed. Opt. Express 2, 1–25.
Altaye, M., Holland, S.K., Wilke, M., Gaser, C., 2008. Infant brain probability templates for MRI segmentation and normalization. Neuroimage 43, 721–730.
American Electroencephalographic Society, 1994. Guideline thirteen: guidelines for standard electrode position nomenclature. American Electroencephalographic Society. J. Clin. Neurophysiol. 11, 111–113.
Amunts, K., Schleicher, A., Zilles, K., 2007. Cytoarchitecture of the cerebral cortex—more than localization. Neuroimage 37, 1061–1065 (discussion 1066–1068).
Arridge, S.R., 1999. Optical tomography in medical imaging. Inverse Prob. 15, R49–R93.
Ashburner, J., Friston, K.J., 1999. Nonlinear spatial normalization using basis functions. Hum. Brain Mapp. 7, 254–266.
Ashburner, J., Andersson, J.L.R., Friston, K.J., 2000. Image registration using a symmetric prior—in three dimensions. Hum. Brain Mapp. 9, 212–225.
Bamett, A.H., Culver, J.P., Sorensen, A.G., Dale, A., Boas, D.A., 2003. Robust inference of baseline optical properties of the human head with three-dimensional segmentation from magnetic resonance imaging. Appl. Opt. 42, 3095–3108.
Bandettini, P.A., 2012. Twenty years of functional MRI: the science and the stories. Neuroimage 62, 575–588.
Barbour, R.L., Graber, H.L., Jenghwa, C., Barbour, S.L.S., Koo, P.C., Aronson, R., 1995. MRI-guided optical tomography: prospects and computation for a new imaging method. IEEE Comput. Sci. Eng. 2, 63–77.
Bluestone, A., Abdoulaev, G., Schmitz, C., Barbour, R., Hielscher, A., 2001. Three-dimensional optical tomography of hemodynamics in the human head. Opt. Express 9, 272–286.
Blume, W.T., Buza, R.C., Okazaki, H., 1974. Anatomic correlates of the ten-twenty electrode placement system in infants. Electroencephalogr. Clin. Neurophysiol. 36, 303–307.
Boas, D.A., Dale, A.M., 2005. Simulation study of magnetic resonance imaging-guided cortically constrained diffuse optical tomography of human brain function. Appl. Opt. 44, 1957–1968.
Boas, D.A., Strangman, G., Culver, J.P., Hoge, R.D., Jasdzewski, G., Poldrack, R.A., Rosen, B.R., Mandeville, J.B., 2003. Can the cerebral metabolic rate of oxygen be estimated with near-infrared spectroscopy? Phys. Med. Biol. 48, 2405–2418.
Boas, D.A., Dale, A.M., Franceschini, M.A., 2004. Diffuse optical imaging of brain activation: approaches to optimizing image sensitivity, resolution, and accuracy. Neuroimage 23 (Supplement 1), S275–S288.
Brett, M., Johnsrude, I.S., Owen, A.M., 2002. The problem of functional localization in the human brain. Nat. Rev. Neurosci. 3, 243–249.
Brodmann, K., 1908. Beiträge zur histologischen Lokalisation der Großhirnrinde. VI: Die Cortexgliederung des Menschen. J. Psychol. Neurol. X, 231–246 (in German).
Burgund, E.D., Kang, H.C., Kelly, J.E., Buckner, R.L., Snyder, A.Z., Petersen, S.E., Schlaggar, B.L., 2002. The feasibility of a common stereotactic space for children and adults in fMRI studies of development. Neuroimage 17, 184–200.
Chance, B., Zhuang, Z., UnAh, C., Alter, C., Lipton, L., 1993. Cognition-activated low-frequency modulation of light absorption in human brain. Proc. Natl. Acad. Sci. U. S. A. 90, 3770–3774.
Chatrian, G.E., 1985. Ten percent electrode system for topographic studies of spontaneous and evoked EEG activity. Am. J. Electroencephalogr. Technol. 25, 83–92.
Collins, D.L., Neelin, P., Peters, T.M., Evans, A.C., 1994. Automatic 3D intersubject registration of MR volumetric data in standardized Talairach space. J. Comput. Assist. Tomogr. 18, 192–205.
Cooper, R.J., Caffini, M., Dubb, J., Fang, Q., Custo, A., Tsuzuki, D., Fischl, B., Wells III, W., Dan, I., Boas, D.A., 2012. Validating atlas-guided DOT: a comparison of diffuse optical tomography informed by atlas and subject-specific anatomies. Neuroimage 62, 1999–2006.
Cox, R.W., 1996. AFNI: software for analysis and visualization of functional magnetic resonance neuroimages. Comput. Biomed. Res. 29, 162–173.
Culver, J.P., Choe, R., Holboke, M.J., Zubkov, L., Durduran, T., Slemp, A., Ntziachristos, V., Chance, B., Yodh, A.G., 2003. Three-dimensional diffuse optical tomography in the parallel plane transmission geometry: evaluation of a hybrid frequency domain/continuous wave clinical system for breast imaging. Med. Phys. 30, 235–247.
Custo, A., Boas, D.A., Tsuzuki, D., Dan, I., Mesquita, R., Fischl, B., Grimson, W.E., Wells III, W., 2010. Anatomical atlas-guided diffuse optical tomography of brain activation. Neuroimage 49, 561–567.
Cutini, S., Scatturin, P., Zorzi, M., 2011. A new method based on ICBM152 head surface for probe placement in multichannel fNIRS. Neuroimage 54, 919–927.
Eggebrecht, A.T., White, B.R., Ferradal, S.L., Chen, C., Zhan, Y., Snyder, A.Z., Dehghani, H., Culver, J.P., 2012. A quantitative spatial comparison of high-density diffuse optical tomography and fMRI cortical mapping. Neuroimage 61, 1120–1128.
Fang, Q., 2010. Mesh-based Monte Carlo method using fast ray-tracing in Plucker coordinates. Biomed. Opt. Express 1, 165–175.